

1 **Carm1 regulates the speed of C/EBP $\alpha$ -induced transdifferentiation by a cofactor stealing**  
2 **mechanism**

3

4 Guillem Torcal Garcia<sup>1,2\*</sup>, Elisabeth Kowenz-Leutz<sup>3\*</sup>, Tian V. Tian<sup>1,2,4\*</sup>, Antonios Klonizakis<sup>1,2</sup>,  
5 Jonathan Lerner<sup>5</sup>, Luisa de Andrés-Aguayo<sup>1,2</sup>, Clara Berenguer<sup>1,2</sup>, Marcos Plana-Carmona<sup>1,2</sup>,  
6 Maria Vila-Casadesús<sup>1,2,4</sup>, Romain Bulteau<sup>6</sup>, Mirko Francesconi<sup>6</sup>, Sandra Peiró<sup>4</sup>, Kenneth S.  
7 Zaret<sup>5</sup>, Achim Leutz<sup>3,7#</sup>, Thomas Graf<sup>1,2#</sup>

8 <sup>1</sup>Gene Regulation, Stem Cells and Cancer Program, Centre for Genomic Regulation (CRG), The  
9 Barcelona Institute of Science and Technology (BIST), Carrer del Doctor Aiguader 88, 08003  
10 Barcelona, Spain

11 <sup>2</sup>Universitat Pompeu Fabra (UPF), Carrer del Doctor Aiguader 88, 08003 Barcelona, Spain.

12 <sup>3</sup>Max Delbrück Center for Molecular Medicine in the Helmholtz Association, Robert-Rössle-  
13 Strasse 10, 13125 Berlin, Germany.

14 <sup>4</sup>Vall d'Hebron Institute of Oncology (VHIO), Carrer de Natzaret 115-117, 08035 Barcelona,  
15 Spain.

16 <sup>5</sup>Institute for Regenerative Medicine and Department of Cell and Developmental Biology,  
17 Perelman School of Medicine, University of Pennsylvania, 3400 Civic Center Blvd, PA 19104  
18 Philadelphia, USA.

19 <sup>6</sup>Laboratoire de Biologie et Modélisation de la Cellule, Université de Lyon, ENS, UCBL, CNRS,  
20 INSERM, UMR5239, U 1210, F-69364 Lyon, France.

21 <sup>7</sup>Institute of Biology, Humboldt University of Berlin, Invalidenstrasse 42, 10115 Berlin, Germany.

22 \*,#Equal contributions

23 Correspondence: [thomas.graf@crg.eu](mailto:thomas.graf@crg.eu); [aleutz@mdc-berlin.de](mailto:aleutz@mdc-berlin.de)

24 **ABSTRACT**

25 Cell fate decisions are driven by lineage-restricted transcription factors but how they are  
26 regulated is incompletely understood. The C/EBP $\alpha$ -induced B cell to macrophage  
27 transdifferentiation (BMT) is a powerful system to address this question. Here we describe that  
28 C/EBP $\alpha$  with a single arginine mutation (C/EBP $\alpha^{R35A}$ ) induces a dramatically accelerated BMT  
29 in mouse and human cells. Changes in the expression of lineage-restricted genes occur as early  
30 as within 1 hour compared to 18 hours with the wild type. Mechanistically C/EBP $\alpha^{R35A}$  exhibits  
31 an increased affinity for PU.1, a bi-lineage transcription factor required for C/EBP $\alpha$ -induced BMT.  
32 The complex induces more rapid chromatin accessibility changes and an enhanced relocation  
33 (stealing) of PU.1 from B cell to myeloid gene regulatory elements. Arginine 35 is methylated by  
34 Carm1 and inhibition of the enzyme accelerates BMT, similar to the mutant. Our data suggest  
35 that the relative proportions of methylated and unmethylated C/EBP $\alpha$  in a bipotent progenitor  
36 can determine the velocity of cell fate choice and lineage directionality.

37

## 38 INTRODUCTION

39 The hematopoietic system is a model of choice to understand how cells diversify into different  
40 lineages (Notta et al., 2016; Orkin and Zon, 2008). Combinations of synergistic and antagonistic  
41 transcription factors (TFs) are the main drivers of cell fate decisions, activating new gene  
42 expression programs while silencing the old ones. Their balance is an important determinant,  
43 with the most highly expressed factors becoming dominant (Graf and Enver, 2009; Okawa et al.,  
44 2018; Orkin and Zon, 2008). However, whether there are other determinants that modulate the  
45 factors' activity and thus the velocity by which a precursor chooses alternative fates remains  
46 poorly understood.

47 A powerful approach to study the mechanism of cell fate decisions is TF-induced lineage  
48 conversions (Graf and Enver, 2009). C/EBP $\alpha$  induces the efficient transdifferentiation of B and T  
49 lineage cells into monocyte/macrophages (henceforth referred as macrophages) (Laiosa et al.,  
50 2006; Xie et al., 2004). This conversion requires the transcription factor PU.1, a key component  
51 of the regulatory networks that define lymphoid and myeloid cells (Arinobu et al., 2007; Leddin et  
52 al., 2011; Singh et al., 1999). C/EBP $\alpha$  contains a C-terminal basic region leucine zipper DNA-  
53 binding domain (bZip) as well as an N-terminal transactivation domain divided into distinct  
54 transactivating elements (TE-I, II and III) (Ramberger et al., 2021). During hematopoiesis it is  
55 most highly expressed in granulocyte-macrophage progenitors (GMPs) (Ohlsson et al., 2016)  
56 and its ablation blocks the formation of GMPs and granulocytes while reducing the number of  
57 monocytes (Heath et al., 2004; Ma et al., 2014; Zhang et al., 2004).

58 Protein post-translational modifications can alter protein structure, subcellular localization and  
59 interactome and may dynamically coordinate signaling networks (Deribe et al., 2010; Torcal  
60 Garcia and Graf, 2021). Arginine methylation is a common protein modification effected by  
61 protein arginine methyltransferases (Prmts), which can catalyze asymmetrical and symmetrical  
62 arginine dimethylation, as well as monomethylation (Wu et al., 2021). While most studies on the  
63 role of arginine methylation have focused on histones it may also affect the function of proteins  
64 involved in DNA replication (Guo et al., 2010) and differentiation (Kawabe et al., 2012; Kowenz-  
65 Leutz et al., 2010). Among the Prmts, Carm1 (Prmt4) is particularly relevant for developmental  
66 decisions such as during early embryo development, adipogenesis and muscle regeneration, as

67 well as for cancer (Kawabe et al., 2012; Kim et al., 2010; Li et al., 2013; M. E. Torres-Padilla et  
68 al., 2007; Yadav et al., 2008).

69 Here we describe that the methylation of a specific arginine within the transcription  
70 activation domain of C/EBP $\alpha$  by the arginine methyltransferase Carm1 dampens the speed by  
71 which the factor induces transdifferentiation. Mechanistically, the unmethylated form of C/EBP $\alpha$   
72 accelerates BMT induction by the enhanced relocation ('stealing) of its partner PU.1 from B cell  
73 gene regulatory regions to myeloid regions, accompanied by an accelerated closing and opening  
74 of chromatin. Our data suggest that the two forms of C/EBP $\alpha$  bias the differentiation of bipotent  
75 progenitors towards alternative lineages.

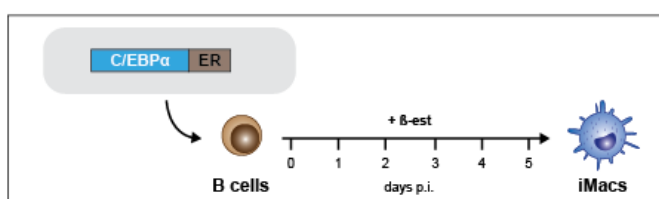
76

## 77 RESULTS

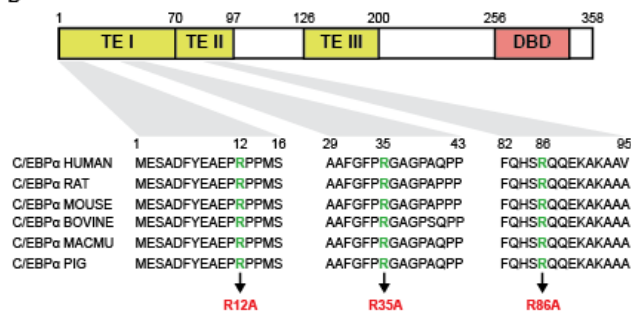
### 78 Mutation of arginine 35 of C/EBP $\alpha$ accelerates immune cell transdifferentiation

79 To identify post-translational modifications that are associated with the BMT-inducing ability of  
80 C/EBP $\alpha$  (**Figure 1A**), we focused on arginines in the factor's transactivation domain. We  
81 identified three evolutionarily conserved arginines (R12, R35, and R86) located within the N-  
82 terminus (**Figure 1B**) in two transactivating elements (TE-I and TE-II) required for efficient BM  
83 (Stoilova et al., 2013). First we generated a triple mutant (C/EBP $\alpha$ <sup>TM</sup>) in which these arginines  
84 were substituted by alanines (Figure 1B) and inserted it into a  $\beta$ -estradiol ( $\beta$ -est)-inducible  
85 retroviral vector (Xie et al., 2004), generating C/EBP $\alpha$ <sup>TM</sup>-ER-GFP. This construct was used to  
86 infect bone marrow-derived B cell precursors (henceforth called B cells) grown on feeder cells  
87 for 2 days and GFP+ B cells isolated. The infected cells were re-seeded on feeders, cultures  
88 treated with  $\beta$ -est and expression of the macrophage marker Mac-1 (CD11b) and the B cell  
89 marker CD19 (Springer et al., 1979; Wang et al., 2012) monitored by FACS at various days later.  
90 Surprisingly, C/EBP $\alpha$ <sup>TM</sup> greatly accelerated BMT, generating almost 100% macrophage-like cells  
91 (Mac-1+, CD19-) within 3 days compared to 4 to 5 days for C/EBP $\alpha$ WT-infected cells (**Figure,**  
92 **1C, S1A**).

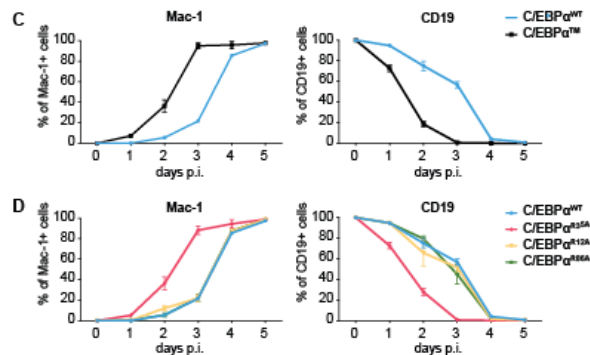
A



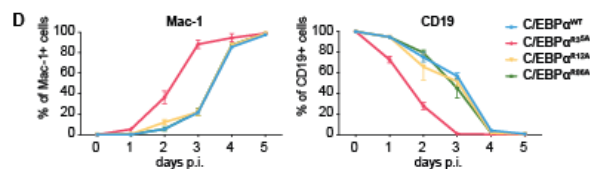
B



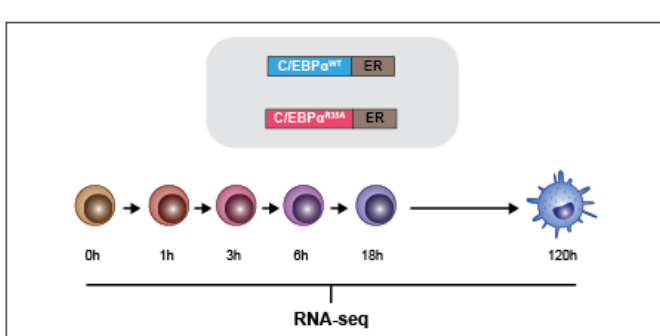
C



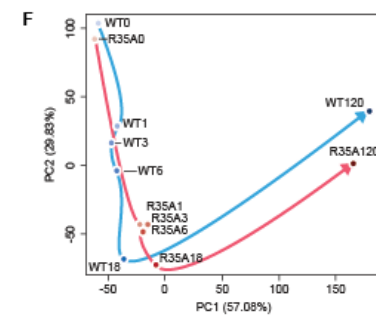
D



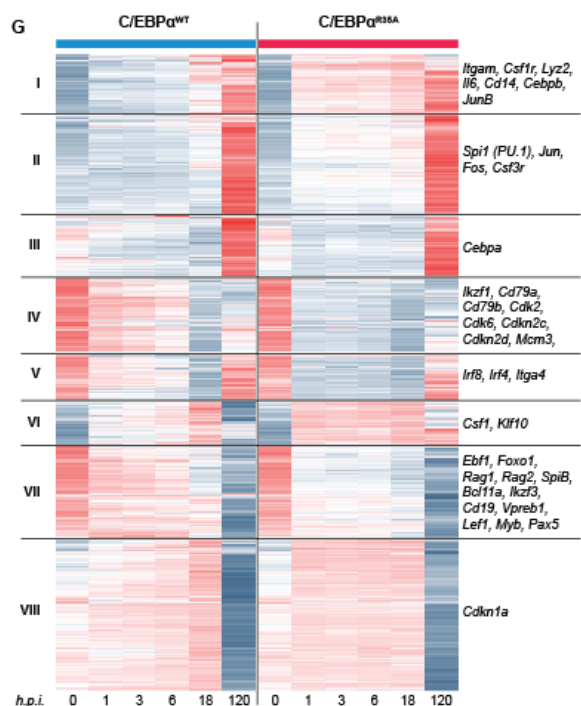
E



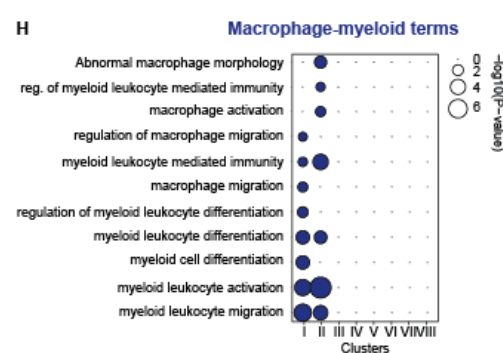
F



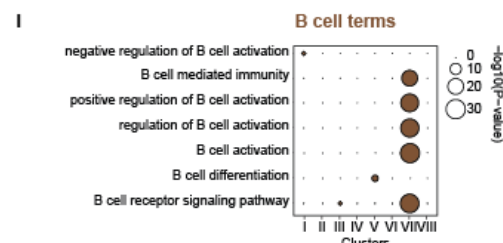
G



H



I



94 **Figure 1. Mutation of arginine 35 in C/EBP $\alpha$  accelerates B cell to macrophage transdifferentiation. A.** Schematics of the B cell to macrophage transdifferentiation (BMT) method. Bone marrow-derived pre-B cells infected with C/EBP $\alpha$ -ER retrovirus are treated with  $\beta$ -est to induce the factor's translocation into the nucleus, inducing a BMT within 4 to 5 days. **B.** C/EBP $\alpha$  structure (TE = transactivation element; DBD = DNA-binding domain) and location of conserved arginines R12, R35, and R86 within the N-terminus, which were replaced by alanines. **C.** Kinetics of BMT induced by wild type (WT) C/EBP $\alpha$  and a triple mutant (C/EBP $\alpha$ <sup>TM</sup>) with alanine replacements of R12, R35 and R86. BMT was assessed by Mac-1 and CD19 expression (mean  $\pm$  s.d., n=3). **D.** Kinetics of BMT induced by C/EBP $\alpha$ <sup>WT</sup> and single arginine to alanine replacements at C/EBP $\alpha$  R12, R35, and R86. **E.** Schematics of experimental approach for RNA-sequencing (RNA-seq) of B cells infected with either C/EBP $\alpha$ <sup>WT</sup>- or C/EBP $\alpha$ <sup>R35A</sup>-ER retroviral constructs induced for various timepoints. **F.** Principal component analysis (PCA) of 11,780 differentially expressed genes (DEGs) during BMT (n=2). Arrows connecting individual time points visualize trajectories **G.** Hierarchical clustering of DEGs with representative genes shown next to each cluster. **H-I.** Gene ontology (GO) enrichment analysis of macrophage-myeloid (**H**) and B cell (**I**) terms of the clusters from Figure 1G. Diameter of circles is proportional to the p-value. See also **Figure S1**.

108 Next, we tested the effect of alanine replacement for each of the 3 individual arginines (R12A, 109 R35A, and R86A) and found that C/EBP $\alpha$ <sup>R35A</sup> recapitulated the phenotype of C/EBP $\alpha$ <sup>TM</sup>, while 110 C/EBP $\alpha$ <sup>R12A</sup> and C/EBP $\alpha$ <sup>R86A</sup> showed no such effect (**Figures 1D, S1A**). Five-day-induced 111 C/EBP $\alpha$ <sup>R35A</sup> cells resembled normal macrophages similar to those seen with C/EBP $\alpha$ <sup>WT</sup> cells, 112 consisting of large, mostly adherent cells, with extensive f-actin filaments and eccentric nuclei. 113 In addition, the cells were highly phagocytic, as >90% of them ingested carboxylated beads 114 (**Figures S1B, C**).

115 These data show that the replacement of arginine 35 with alanine in C/EBP $\alpha$  dramatically 116 accelerates the factor's capacity to induce a BMT, as evidenced by a higher velocity of silencing 117 and activation of B cell and macrophage markers, respectively. Moreover, the induced cells 118 resembled normal macrophages and were functional.

119 **C/EBP $\alpha$ <sup>R35A</sup> hastens gene expression changes of lineage-associated genes at early time 120 points**

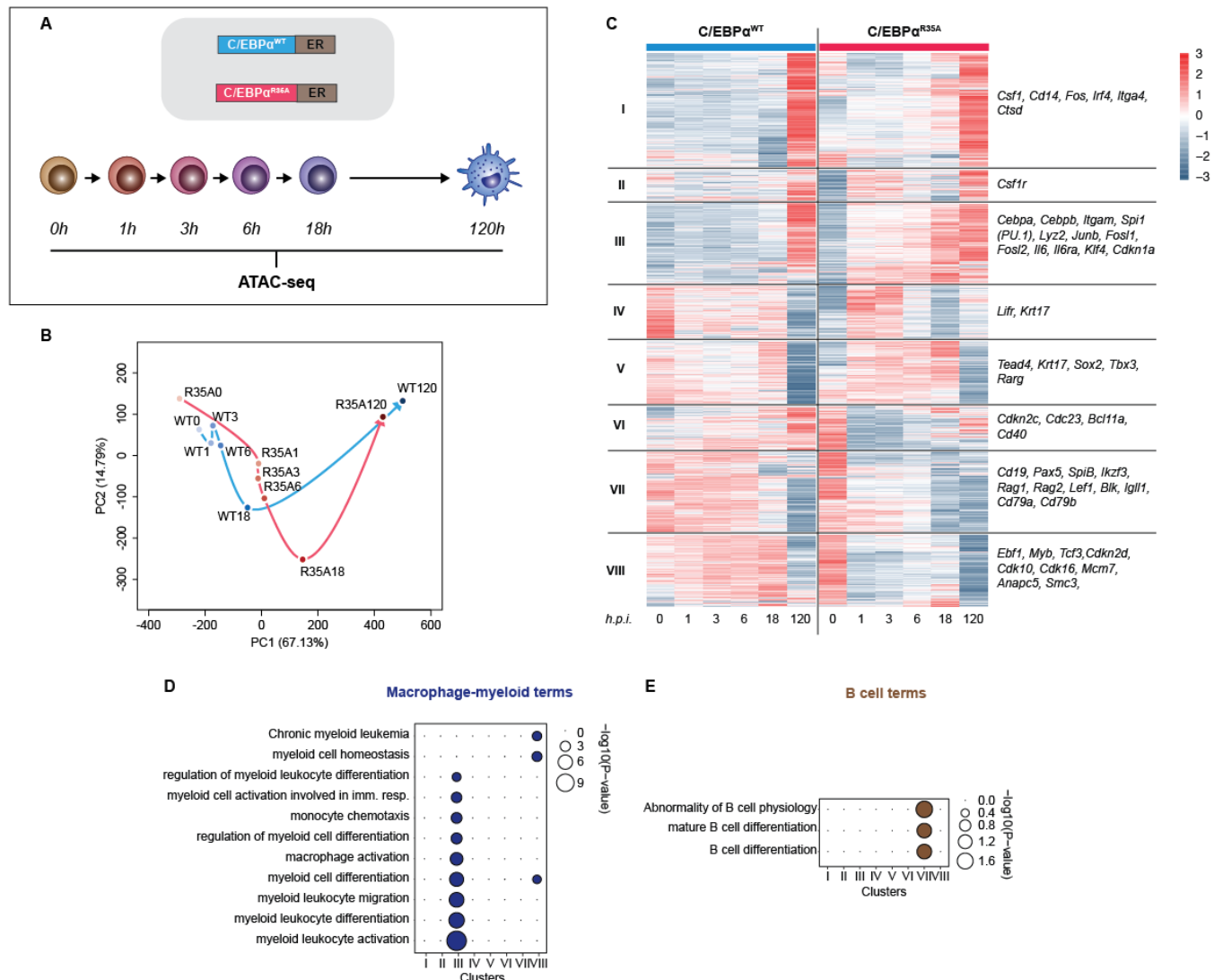
121 To study the effects of C/EBP $\alpha$ <sup>R35A</sup> on gene expression, we performed RNA-sequencing 122 (RNA-seq) of infected B cells induced for 0, 1, 3, 6, 18, and 120 hours (**Figure 1E**). Principal 123 component analysis (PCA) showed a pronounced acceleration in the trajectory of differentially 124 expressed genes throughout BMT (11,780 genes) compared to the WT virus. Strikingly, induction 125 of C/EBP $\alpha$ <sup>R35A</sup> cells for just 1 hour caused changes similar to 18 hours induced C/EBP $\alpha$ <sup>WT</sup> cells,

126 with their trajectories converging again at 120 hours post induction (hpi; **Figure 1F**). The vast  
127 majority of genes affected by the wild type and the mutant exhibited similar expression levels at  
128 the endpoint of the conversion, indicating that the mutant mostly accelerates the speed of BMT  
129 without inducing an aberrant phenotype (**Figure S1D**). Moreover, the largest differences in gene  
130 expression values between wild type and mutant cells were observed at 1 and 3 hpi (**Figure**  
131 **S1D**). Hierarchical clustering of all the 11,780 differentially expressed genes throughout BMT  
132 yielded 8 clusters (**Figure 1G**). These could be separated into two large groups, with genes in  
133 clusters I, II, IV and VIII displaying faster activation by C/EBP $\alpha$ <sup>R35A</sup>, while clusters IV, V and VII  
134 showed faster silencing. Macrophage-myeloid related GO terms were enriched in clusters I and  
135 II (**Figures 1H, S1F**) and included the myeloid-restricted genes *Itgam* (encoding Mac-1) *Lyz2*  
136 (lysozyme), *Csf1r* (M-CSF receptor) and *Cd14* (**Figures 1G, S1G**). Conversely, B cell-related  
137 GO terms were enriched in cluster VII (**Figures 1I, S1F**) and included the B cell-restricted genes  
138 *Cd19*, *Pax5*, *Ebf1* and *Rag2* (**Figures 1G, S1G**). The kinetics of individual macrophage and B  
139 cell-associated genes (**Figure S1H**) further illustrate the C/EBP $\alpha$ <sup>R35A</sup>-induced BMT acceleration.

140 These results extend the findings obtained with B cell and macrophage cell surface markers  
141 to thousands of differentially regulated lineage-associated genes. The most dramatic differences  
142 in gene expression changes induced by C/EBP $\alpha$ <sup>R35A</sup> occurred within 3 hpi and then converged  
143 again at 120 hpi.

144 **C/EBP $\alpha$ <sup>R35A</sup> accelerates chromatin remodelling at regulatory elements of lineage-  
145 restricted genes**

146 Major gene expression changes are typically associated with extensive chromatin remodeling  
147 (Klemm et al., 2019). To study changes in chromatin accessibility occurring during BMT, we  
148 performed assays for Transposase-Accessible Chromatin using sequencing (ATAC-seq) at  
149 various time points after C/EBP $\alpha$ <sup>WT</sup> and C/EBP $\alpha$ <sup>R35A</sup> induction (**Figure 2A**).



150

151 **Figure 2. C/EBP $\alpha$ <sup>R35A</sup> accelerates chromatin accessibility at gene regulatory elements of lineage-restricted**

152 genes. A. Experimental approach used for chromatin accessibility profiling. B cells infected with either C/EBP $\alpha$ <sup>WT</sup>-

153 ER or C/EBP $\alpha$ <sup>R35A</sup>-ER retroviral constructs (n=2 biological replicates) were induced for the indicated times and

154 processed for ATAC-seq. B. PCA of differential chromatin accessibility dynamics during BMT induced by C/EBP $\alpha$ <sup>WT</sup>

155 (cyan) or C/EBP $\alpha$ <sup>R35A</sup> (magenta), based on 91,830 ATAC-seq peaks differentially called for the two conditions.

156 Arrows connecting individual timepoints show trajectories. C. Hierarchical clustering of differentially accessible

157 promoters (14,233 peaks) with representative genes shown next to each cluster. D-E. Gene ontology analysis of

158 macrophage-myeloid (D) and B cell (E) terms of each cluster. Diameter of circles is proportional to the p-value. See

159 also Figure S2.

160 ATAC-seq revealed 91,830 peaks significantly different between wild type and mutant cells in at

161 least one time point, indicating differential chromatin accessibility. These regions fell into three

162 groups: a) faster opening Gene Regulatory Elements (GREs), with highest peaks at 120hpi

163 (43,429 peaks); b) faster closing GREs, with highest peaks at 0 hpi (36,380 peaks) and c)  
164 transiently opening GREs with highest peaks at 18 hpi (12,021 peaks) (**Figure S2A, B**). While  
165 both opening and closing GREs showed a largely accelerated trend with C/EBP $\alpha$ <sup>R35A</sup>, transiently  
166 opening GREs showed only subtle differences between the two conditions (**Figure S2B**). PCA  
167 analysis of the differential ATAC peaks revealed an acceleration of chromatin accessibility by  
168 C/EBP $\alpha$ <sup>R35A</sup> (**Figure 2B**), with values of the 1-6 hpi C/EBP $\alpha$ <sup>R35A</sup> samples resembling the 18 hpi  
169 C/EBP $\alpha$ <sup>WT</sup> sample.

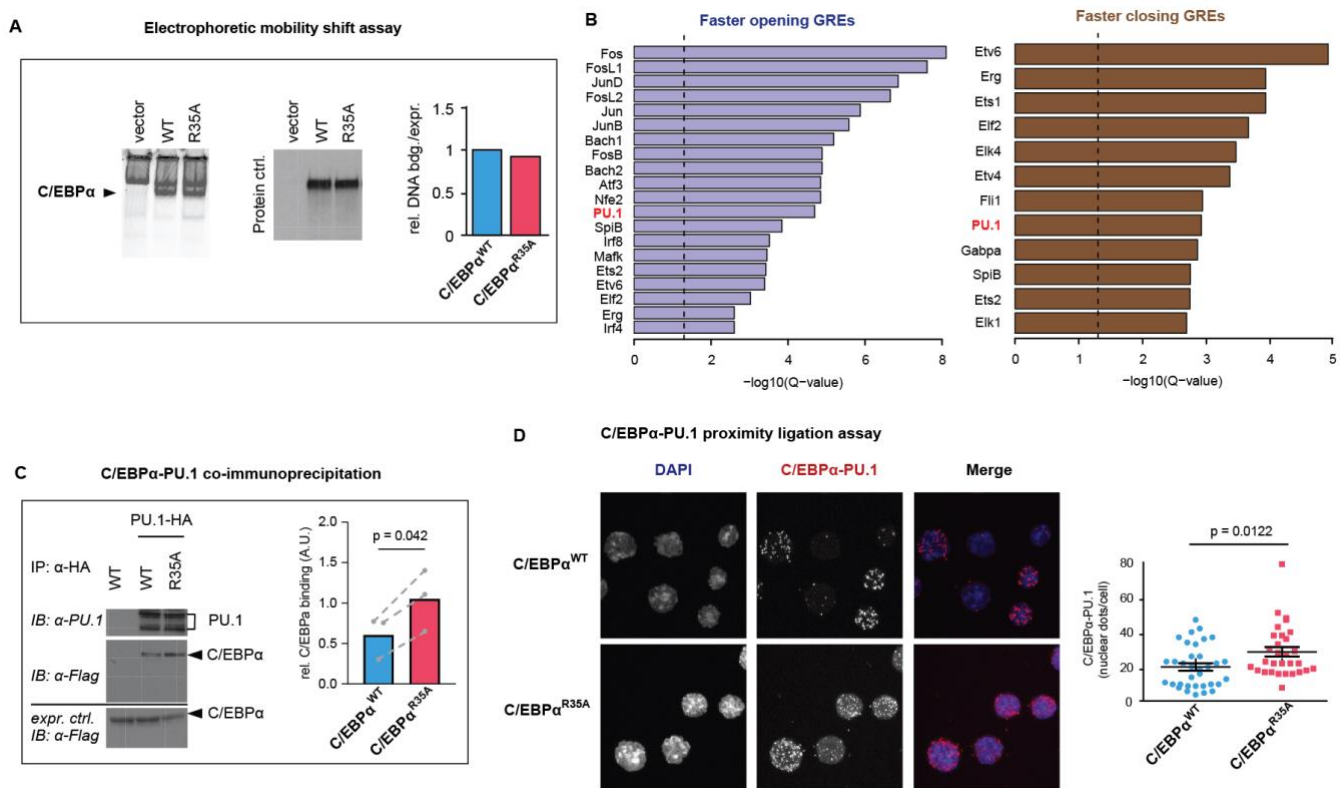
170 We then grouped the 14,233 differential peaks at promoter regions into eight clusters, with  
171 genes in clusters I, II and III exhibiting opening dynamics dramatically accelerated by  
172 C/EBP $\alpha$ <sup>R35A</sup>, while genes in clusters VII and VIII showing accelerated closing (**Figure 2C**). GO  
173 analysis revealed an enrichment of macrophage terms for cluster III (**Figure 2D**) and included  
174 the macrophage-restricted genes *Itgam* and *Lyz2* (**Figure 2C**). Quantification of accessibility  
175 changes in GREs (including promoters and enhancers of genes) in this cluster showed an  
176 accelerated chromatin opening by C/EBP $\alpha$ <sup>R35A</sup> at the early timepoints (exemplified by *Itgam* and  
177 *Lyz2* in **Figure S2C**). Conversely, the faster closing GREs in cluster VIII were enriched for B cell-  
178 related GO terms and included the B cell genes *Cd19*, *Pax5* and *Rag2* (**Figures 2C, E, S2D**).  
179 Differences in chromatin accessibility at these clusters were no longer apparent at 120 hpi  
180 (**Figures 2B, C**).

181 Overall, these results indicate that C/EBP $\alpha$ <sup>R35A</sup> is more efficient at inducing chromatin opening  
182 or closing at lineage-specific GREs compared to C/EBP $\alpha$ <sup>WT</sup>, consistent with the observed  
183 acceleration of gene expression changes (**Figure 1E-I**). Again, these differences are most  
184 pronounced at the earliest time points.

### 185 **Differentially opening and closing chromatin regions are enriched for PU.1 motif**

186 To test whether the accelerated changes in chromatin accessibility are due to differential DNA  
187 binding affinities, we performed an electrophoretic mobility shift assay with both proteins, using  
188 nuclear extracts from HEK-293T cells expressing either C/EBP $\alpha$ <sup>WT</sup> or C/EBP $\alpha$ <sup>R35A</sup>. These were  
189 incubated with an end-labeled oligonucleotide containing a palindromic C/EBP $\alpha$ -binding motif  
190 and run on a native acrylamide gel. The intensity of the resulting bands corresponding to

191 C/EBP $\alpha$ <sup>WT</sup> and C/EBP $\alpha$ <sup>R35A</sup> complexes were similar, indicating that the mutation does not  
 192 significantly affect the DNA-binding capacity of the factor (Figure 3A).



193

194 **Figure 3. C/EBP $\alpha$ <sup>R35A</sup> exhibits an increased affinity for PU.1.** **A.** Electrophoretic mobility shift assay with nuclear  
 195 extracts of HEK-293T cells transfected with either C/EBP $\alpha$ <sup>WT</sup> or C/EBP $\alpha$ <sup>R35A</sup> incubated with a fluorophore-labeled  
 196 oligonucleotide containing a palindromic C/EBP $\alpha$ -binding motif (left). Protein expression control of nuclear C/EBP $\alpha$   
 197 proteins by western blot (middle) and densitogram-based relative DNA binding versus protein expression (right). **B.**  
 198 Lists of the top *de novo* motifs in faster opening or closing GREs induced by C/EBP $\alpha$ <sup>R35A</sup> (Figures S2A, B), with the  
 199 PU.1 motif indicated in red. Dashed lines correspond to the significance threshold of Q-value ( $\leq 0.05$ ). **C.** Co-  
 200 immunoprecipitation of PU.1 and C/EBP $\alpha$  in HEK-293T cells transfected with either C/EBP $\alpha$ <sup>WT</sup> or C/EBP $\alpha$ <sup>R35A</sup> (left)  
 201 and quantification of interaction of three independent experiments (right). Values shown were normalized to the  
 202 expression of C/EBP $\alpha$  (mean + individual values). Dashed lines indicate paired values; statistical significance was  
 203 determined using a paired Student's t-test. **D.** Proximity ligation assay of C/EBP $\alpha$  and PU.1 in mouse B cells induced  
 204 with either C/EBP $\alpha$ <sup>WT</sup> or C/EBP $\alpha$ <sup>R35A</sup> for 24 hours. On the left, confocal microscopy images of the cells showing  
 205 nuclear dots. On the right, quantification of interactions by counting nuclear dots per cell (mean  $\pm$  s.e.,  $n=30-34$ ;  
 206 statistical significance determined using an unpaired Student's t-test). See also Figure S3.

207 Another possibility is that the altered chromatin remodeling capacity of C/EBP $\alpha$ <sup>R35A</sup> is due to  
 208 the differential interaction with another protein(s). In an attempt to find such potential interactors,

209 we performed a *de novo* motif discovery analysis with the differentially accessible GREs in the  
210 three groups by matching them against known TF motifs (**Figure S2A** and **B**). Faster and  
211 transiently opening GREs were found to be strongly enriched for AP-1/leucine zipper family TF  
212 motifs (c-Fos, c-Jun and JunB), a family of factors known to be able to heterodimerize with  
213 C/EBP $\alpha$  to activate myeloid genes (Cai et al., 2008). In contrast, faster closing GREs were mostly  
214 enriched for ETS family TF motifs such as Ets1, Fli1, SpiB and Gabpa, known to be associated  
215 with B cell lineage differentiation and function (Eyquem et al., 2004; Hu et al., 2001; Xue et al.,  
216 2007; Zhang et al., 2008). Several motifs were also enriched in both the accelerated chromatin  
217 opening and closing groups, including that of PU.1 and the closely related factor Spi-B (**Figures**  
218 **3B, S3A**). Conversely, the transiently opening regions were enriched for AP-1 motifs but not for  
219 PU.1 (**Figure S3B**).

220 These observations show that chromatin regions more rapidly opened by C/EBP $\alpha^{R35A}$  are  
221 enriched for AP-1 family binding motifs in line with the synergism between C/EBP $\alpha$  and AP-1  
222 family factors during myeloid differentiation (Cai et al., 2008). Conversely, the association of Ets  
223 family motifs with more rapidly closed regions might reflect the role of Fli1, Spi-B and in B cell  
224 differentiation (Zhang et al., 2008). That the PU.1 motif is shared between faster opening and  
225 closing regions might reflect its dual roles in the two lineages (Scott et al., 1994; Singh et al.,  
226 1999).

## 227 **C/EBP $\alpha^{R35A}$ exhibits an increased affinity for PU.1**

228 Since PU.1 is a necessary partner of C/EBP $\alpha$  during myeloid cell specification (Heinz et al., 2010;  
229 van Oevelen et al., 2015; Xie et al., 2004) in the following we focused on the role of PU.1 during  
230 BMT. To test whether arginine 35 modulates the interaction of C/EBP $\alpha$  with PU.1, we performed  
231 co-immunoprecipitation experiments with cellular extracts from HEK293-T cells co-transfected  
232 with PU.1 and either WT or mutant C/EBP $\alpha$ . This revealed an approximately 2-fold increase in  
233 the interaction between C/EBP $\alpha^{R35A}$  and PU.1 compared to C/EBP $\alpha^{WT}$  (**Figure 3C**). Also,  
234 proximity ligation assays showed a stronger interaction between PU.1 and C/EBP $\alpha^{R35A}$   
235 compared to C/EBP $\alpha^{WT}$ , as determined by a significantly higher number of fluorescent nuclear  
236 dots (**Figure 3D**). These results therefore indicate that a mutation of C/EBP $\alpha^{R35}$  increases the  
237 factor's affinity for its obligate partner PU.1.

## 238 **C/EBP $\alpha^{R35A}$ shows an increased synergy with PU.1 in fibroblasts**

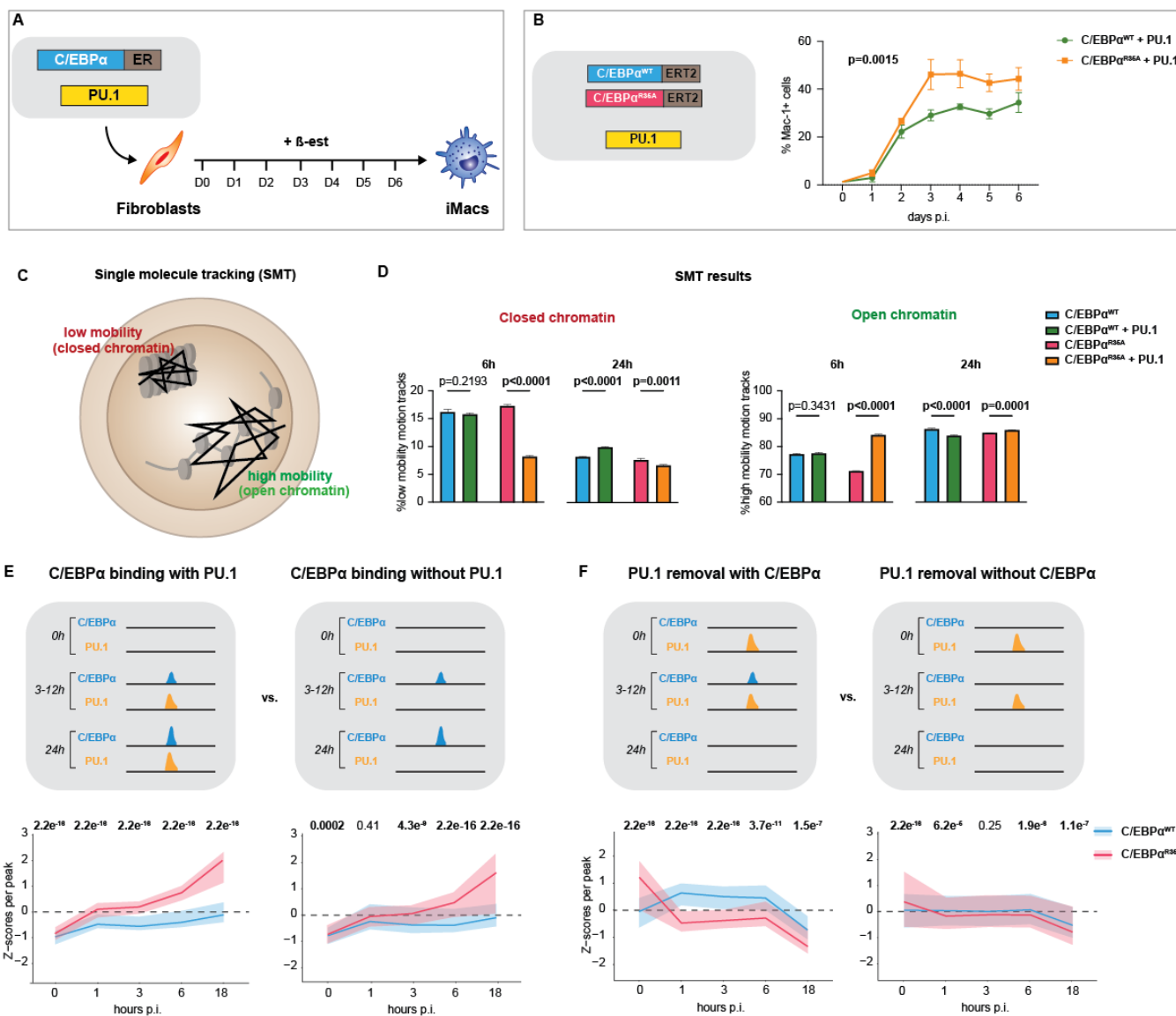
239 We have previously shown that C/EBP $\alpha$  synergizes with PU.1 in converting NIH 3T3 fibroblasts  
240 into macrophage-like cells (Feng et al., 2008a) (**Figure 4A**). Therefore, to determine how the  
241 mutant behaves in this system, we generated NIH 3T3-derived cell lines (3T3aER-R and  
242 3T3aER-A) stably expressing inducible forms of C/EBP $\alpha$ <sup>WT</sup> or C/EBP $\alpha$ <sup>R35A</sup>, respectively. These  
243 lines were then infected with a constitutive PU.1 retroviral construct, treated with  $\beta$ -est, and Mac-  
244 1 levels monitored by FACS at various times post-induction. As described earlier (Feng et al.,  
245 2008b), the combination of C/EBP $\alpha$ <sup>WT</sup> with PU.1 activated Mac-1 expression while the individual  
246 constructs did not (**Figures 4B, S4A, B**). Importantly, C/EBP $\alpha$ <sup>R35A</sup> synergized with PU.1 more  
247 strongly than C/EBP $\alpha$ <sup>WT</sup> in activating Mac-1 (**Figures 4B, S4A**). In addition, cells co-expressing  
248 PU.1 and C/EBP $\alpha$ <sup>R35A</sup> exhibited dramatic morphological changes, with cells co-expressing PU.1  
249 and C/EBP $\alpha$ <sup>WT</sup> displaying more subtle alterations (**Figure S4C**).

250 **Single-molecule tracking experiments in fibroblasts show a PU.1-enhanced chromatin  
251 opening by C/EBP $\alpha$ <sup>R35A</sup>**

252 To explore whether also in fibroblasts the two forms of C/EBP $\alpha$  exhibit differences in  
253 chromatin opening and how this is influenced by PU.1, we performed single-molecule tracking  
254 (SMT) experiments. This allows to visualize the Brownian-like movement of individual TF  
255 molecules and their interaction with open and closed chromatin (Lerner et al., 2020; Liu and  
256 Tjian, 2018) (**Figure 4C**). For this purpose, we generated NIH3T3 cells expressing doxycycline-  
257 inducible Halo-tagged histone H2B, C/EBP $\alpha$ <sup>WT</sup> or C/EBP $\alpha$ <sup>R35A</sup>. After induction for either 6h or 24h  
258 these cells were used to perform SMT on ~50 cells per condition and 20,000 single-molecule  
259 motion tracks were randomly down-sampled in triplicates to compare each condition (Chen et  
260 al., 2014). Monitoring the radius of confinement and average displacement of histone H2B  
261 allowed us to define low and high mobility chromatin, corresponding to closed and open states,  
262 respectively (Lerner et al., 2020) (**Figure S4D**).

263 Similar two-parameter assessment of motion tracks of C/EBP $\alpha$ <sup>WT</sup> and C/EBP $\alpha$ <sup>R35A</sup> showed  
264 that after 6 hpi, both TFs display interactions with low mobility (closed) chromatin, with  
265 C/EBP $\alpha$ <sup>R35A</sup> showing a slightly increased interaction (**Figure 4D**). This observation is consistent  
266 with the elevated affinity for nucleosomes of C/EBP $\alpha$  measured *in vitro* (Fernandez Garcia et al.,  
267 2019; Lerner et al., 2020). At 24 hpi, both C/EBP $\alpha$ <sup>WT</sup> and C/EBP $\alpha$ <sup>R35A</sup> showed a decreased  
268 interaction with low mobility chromatin and increased interaction with high mobility chromatin

269 **(Figure 4D).** This transition to higher mobility chromatin suggests an opening of regions bound  
 270 by C/EBP $\alpha$ , consistent with the known pioneering function of C/EBP $\alpha$  (Fernandez Garcia et al.,  
 271 2019).



272  
 273 **Figure 4. C/EBP $\alpha$ <sup>R35A</sup> shows an enhanced synergy with PU.1 and hastens its relocation from B cell to myeloid**  
 274 **GREs.** **A.** Schematic representation of TF-induced fibroblast to macrophage transdifferentiation. NIH3T3 fibroblasts  
 275 were infected C/EBP $\alpha$ <sup>WT</sup>-ER or C/EBP $\alpha$ <sup>R35A</sup>-ER in the presence or absence of PU.1 construct. Cells were induced  
 276 with  $\beta$ -est for the indicated times, causing a conversion to macrophage- like cells (iMacs) within 6 days p.i. **B.**  
 277 Kinetics of Mac-1 expression (mean  $\pm$  s.d., n=3; statistical significance was determined using two-way ANOVA). **C.**  
 278 Schematic representation of single molecule movements of TFs bound to closed (low mobility) or open (high  
 279 mobility) chromatin. **D.** Quantification of single cell motion tracks (mean  $\pm$  s.d., n=3 x 20,000 randomized down  
 280 sampled motion tracks; statistical significance determined using two-way ANOVA with multiple comparisons). **E, F.**

281 Virtual chromatin immunoprecipitation of C/EBP $\alpha$  and PU.1 during BMT induced either by C/EBP $\alpha$ <sup>WT</sup> or C/EBP $\alpha$ <sup>R35A</sup>  
282 for the indicated times, showing schematics of peaks illustrating the different conditions tested. **E**, Selected regions  
283 corresponding to sites that are devoid of C/EBP $\alpha$  and PU.1 in B cells and become bound by both factors (left) or  
284 only by C/EBP $\alpha$  (right) throughout BMT. **F** Selected regions corresponding to sites where PU.1 is bound in B cells  
285 and either removed by transient binding of C/EBP $\alpha$  (left) or by another mechanism during BMT (right). See also  
286 **Figure S4**. Data were computed from ATAC-seq experiments (**Figure 2**) and from ChIP-seq of C/EBP $\alpha$  and PU.1  
287 in B cells induced with  $\beta$ -est for 0, 3, 12 and 24 hours (van Oevelen et al., 2015). Plots on the bottom show chromatin  
288 accessibility Z-scores per ATAC peak of B cells induced with either wild type (cyan) or mutant C/EBP $\alpha$  (magenta)  
289 at different hpi (line=median; shaded background=IQR; statistical significance was determined using a Wilcoxon  
290 signed-rank test).

291 We then tested the effect of PU.1 co-expression on interactions of C/EBP $\alpha$  with open or  
292 closed chromatin. At 6 hpi C/EBP $\alpha$ <sup>R35A</sup> cells co-expressing PU.1 displayed a dramatic decrease  
293 in interaction with low mobility chromatin concomitantly with increased interaction with higher  
294 mobility chromatin, while PU.1 co-expression had little effect on the mobility of C/EBP $\alpha$ <sup>WT</sup>. This  
295 suggests a faster chromatin opening by C/EBP $\alpha$ <sup>R35A</sup> at sites bound by PU.1 (**Figure 4D** and **F**).  
296 The observed differences between C/EBP $\alpha$ <sup>WT</sup> and C/EBP $\alpha$ <sup>R35A</sup> co-expressing PU.1 essentially  
297 disappeared after 24h, suggesting that the two protein complexes open closed chromatin at  
298 different speeds but reach similar endpoints (**Figure 4D** and **E**).

299 Altogether these results show that in 3T3 cells C/EBP $\alpha$ <sup>R35A</sup> displays an enhanced  
300 synergism with PU.1 in that the complex induces a faster chromatin opening than the C/EBP $\alpha$ <sup>WT</sup>-  
301 PU.1 complex, coincident with stronger activation of macrophage markers and induced cell  
302 morphology changes.

### 303 **C/EBP $\alpha$ <sup>R35A</sup> hastens the relocation of PU.1 from B cell to macrophage enhancers during 304 BMT induction**

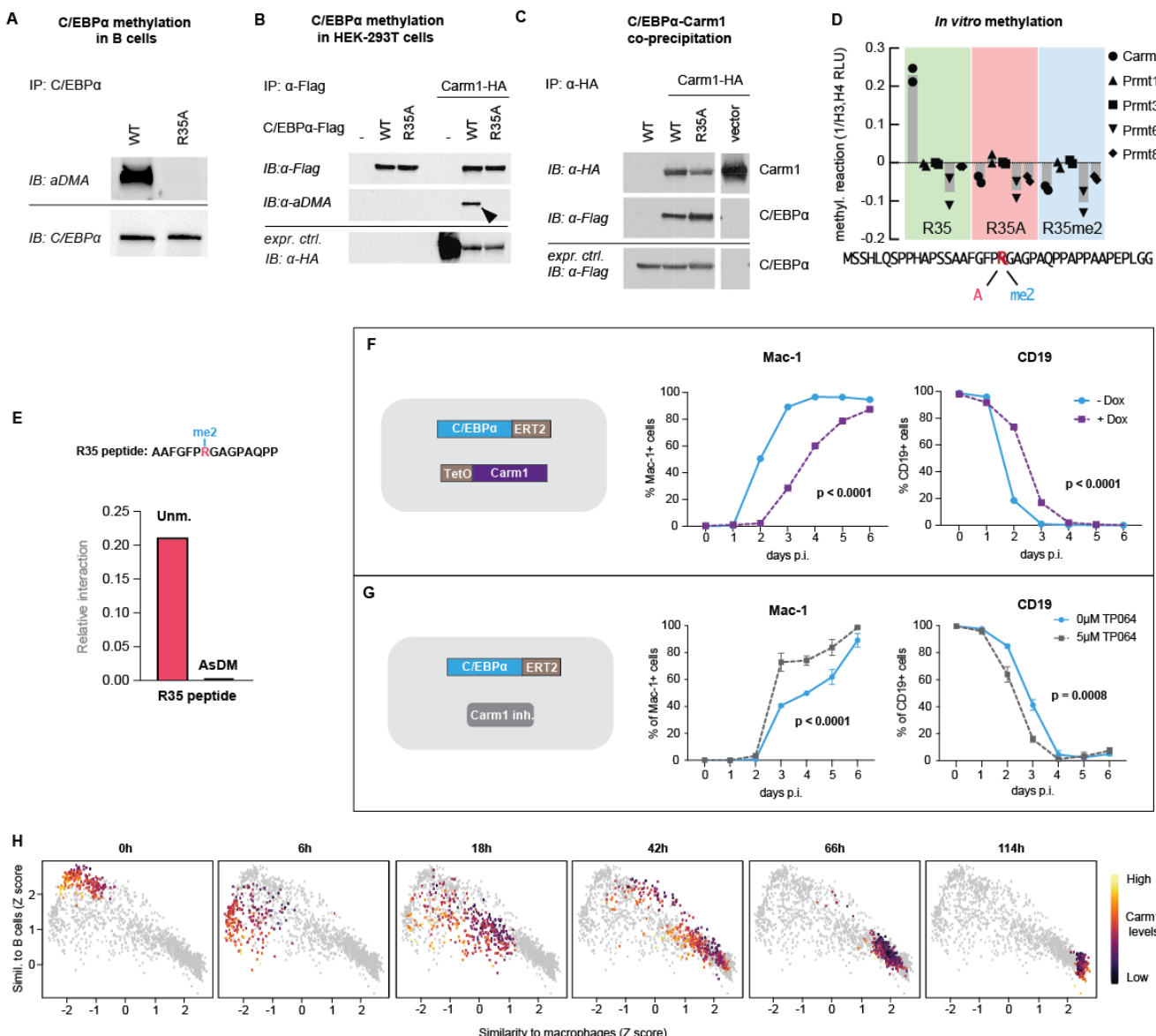
305 The data described raised the possibility that C/EBP $\alpha$  causes a relocation of PU.1 from B cell to  
306 macrophage regulatory regions and that the mutant, through its enhanced interaction with PU.1,  
307 is more efficient at doing so. This hypothesis predicts that C/EBP $\alpha$ <sup>R35A</sup> binding to GREs occupied  
308 by PU.1 should induce stronger changes in chromatin accessibility than C/EBP $\alpha$ <sup>WT</sup>, while sites  
309 devoid of PU.1 should behave more similarly. To test this, we performed a virtual ChIP-seq  
310 analysis of C/EBP $\alpha$  and PU.1 during BMT, combining previously generated ChIP-seq data (van  
311 Oevelen et al., 2015) with our new ATAC-seq data. We first identified regions stably bound by  
312 C/EBP $\alpha$  throughout BMT and then distinguished sites already occupied by PU.1 from PU.1-free

313 sites. This revealed that C/EBP $\alpha^{R35A}$  induces a significant acceleration of chromatin *opening* at  
314 PU.1-bound regions compared to C/EBP $\alpha^{WT}$ , while regions bound by C/EBP $\alpha$  alone showing  
315 much smaller differences (**Figure 4E**). Next, we focused on sites where PU.1 is removed by  
316 transiently bound by C/EBP $\alpha$ , distinguishing them from sites where PU.1 is removed yet no  
317 C/EBP $\alpha$  binding was detected at any timepoint. This showed that transient binding of C/EBP $\alpha^{R35A}$   
318 accelerated PU.1 displacement and chromatin closing at PU.1-bound regions. In contrast,  
319 although PU.1 was also still removed at sites not targeted by C/EBP $\alpha$ , the effect was much milder  
320 (**Figure 4F**).

321 Altogether, our results are consistent with the hypothesis that during BMT, C/EBP $\alpha$  ‘steals’  
322 endogenous PU.1 from B cell GREs and relocates it to myeloid GREs. This stealing is  
323 exacerbated by C/EBP $\alpha^{R35A}$ , which is able to more efficiently relocate PU.1 and thus accelerate  
324 the conversion of PU.1 from a B cell regulator to a myeloid regulator, in line with the SMT results  
325 obtained in fibroblasts.

326 **Carm1 asymmetrically dimethylates arginine 35 of C/EBP $\alpha$  and decreases its affinity for**  
327 **PU.1**

328 The finding that a mutation in a specific arginine of C/EBP $\alpha$  is responsible for the observed  
329 BMT acceleration raised the possibility that the phenotype is caused by the loss of its potential  
330 to be methylated. Since asymmetric dimethylation is one of the most common arginine  
331 modifications (Bedford and Clarke, 2009; Bedford and Richard, 2005), we first determined  
332 whether R35 is asymmetrically dimethylated. To this end, we generated two cell lines named  
333 BLaER2 and BLaER2-A, derived from the B-ALL line RCH-ACV (Jack et al., 1986) expressing  
334 the 4-hydroxytamoxifen (4-OHT)- inducible constructs C/EBP $\alpha^{WT}$ -ERT2 and C/EBP $\alpha^{R35A}$ -ERT2,  
335 respectively. We then induced these cells for 24h with 4-OHT, immunoprecipitated C/EBP $\alpha$ , and  
336 ran a Western with an antibody specific for asymmetrically dimethylated arginine (aDMA)-  
337 containing proteins. The antibody detected C/EBP $\alpha^{WT}$  but not C/EBP $\alpha^{R35A}$ , thus revealing that  
338 arginine 35 is asymmetric dimethylated (**Figure 5A**). We next co-transfected HEK293-T cells  
339 with either C/EBP $\alpha^{WT}$  or C/EBP $\alpha^{R35A}$  and several type I Prmts, namely Prmt1, 3, 4 (Carm1) and  
340 6; and assessed the methylation status of C/EBP $\alpha$ . Only Carm1 was able to induce methylation  
341 of C/EBP $\alpha^{WT}$  while C/EBP $\alpha^{R35A}$  remained unmethylated (**Figures 5B, S5A**).



342

343 **Figure 5. Carm1 asymmetrically dimethylates arginine 35 and regulates the speed of C/EBP $\alpha$ -induced BMT.**

344 A. Immunoprecipitation (IP) and immunoblotting (IB) of C/EBP $\alpha$  and asymmetrically dimethylated arginine (aDMA)

345 containing proteins. B. Immunoprecipitation of C/EBP $\alpha$  from HEK293T cells co-transfected with either C/EBP $\alpha$ <sup>WT</sup>-

346 Flag or C/EBP $\alpha$ <sup>R35A</sup>-Flag with or without Carm1-HA, followed by immunoblot with antibodies against aDMA, Flag

347 and HA. C. Immunoprecipitation of Carm1 from HEK293T cells co-transfected with either C/EBP $\alpha$ <sup>WT</sup>-Flag or

348 C/EBP $\alpha$ <sup>R35A</sup>-Flag and Carm1-HA, followed by immunoblot with antibodies against Flag and HA. D. In vitro

349 methylation assays with recombinant Carm1, Prmt1, Prmt3, Prmt6 or Prmt8 proteins together with C/EBP $\alpha$  peptides

350 (aa 15-54) that contain either unmethylated arginine 35 (green), with an alanine replacement (A, magenta), or

351 asymmetrically dimethylated (me2, cyan) (mean and individual values are displayed, n=2). E. Interaction with PU.1

352 of a 14-mer peptide (top) containing either an unmethylated (Unm.) or an asymmetrically dimethylated arginine (me,

353 AsDM). The data were extracted from (Ramberger et al., 2021). F. Effect of Carm1 overexpression on BMT kinetics

354 of human B cells measured by Mac-1 and CD19 expression (mean  $\pm$  s.d., n=3, statistical significance was  
355 determined using two-way ANOVA). **G.** Same as F, but effect of Carm1 inhibition by 5 $\mu$ M of TP064. **H.** Correlation  
356 of Carm1 expression levels in single cell trajectories with B cell and macrophage states. Data extracted from  
357 previously published work (Francesconi et al., 2019).

358 To rule out the possibility that the R35 mutation is impaired in its interaction with Carm1 we  
359 performed Co-IP experiments in HEK293-T cells co-transfected with Carm1 and either  
360 C/EBP $\alpha$ <sup>WT</sup> or C/EBP $\alpha$ <sup>R35A</sup>, which showed that both proteins are able to interact with the enzyme  
361 (**Figure 5C**). To quantitatively assess the interaction of C/EBP $\alpha$ <sup>WT</sup> and C/EBP $\alpha$ <sup>R35A</sup> with Carm1  
362 we performed a PLA assay. For this, NIH3T3 cell lines carrying ER fusions of C/EBP $\alpha$ <sup>WT</sup> and  
363 C/EBP $\alpha$ <sup>R35A</sup> were induced with  $\beta$ -est for 24 hours and subjected to the assay, involving staining  
364 with antibodies to C/EBP $\alpha$  and PU.1. We observed nuclear dots in both lines, with slightly higher  
365 numbers in C/EBP $\alpha$ <sup>R35A</sup> cells, supporting the notion that both forms of C/EBP $\alpha$  can interact with  
366 Carm1 (**Figure S5B**).

367 To further assess the enzyme's specificity, we performed an *in vitro* methylation assay using  
368 synthetic peptides (10-14-mers), covering all 20 arginine residues of C/EBP $\alpha$ . Only the peptide  
369 containing arginine 35 showed a methylation signal (**Figure S5C**). We also performed an *in vitro*  
370 methylation assay using a C/EBP $\alpha$  peptide spanning amino acids 15-54 and containing either  
371 unmethylated R35, asymmetrically di-methylated R35 or an alanine replacement in the presence  
372 of either Carm1, Prmt1, Prmt3, Prmt6 or Prmt8. Only Carm1 was able to methylate the peptide  
373 with the original arginine, while no methylation was detected with the other Prmts and with  
374 peptides containing methylated R35 or an alanine replacement (**Figure 5D**). Finally, we  
375 investigated whether the methylation status of C/EBP $\alpha$  affects its affinity for PU.1, analyzing the  
376 interaction data from a peptide motif-based C/EBP $\alpha$  interactome screen (Protein interaction  
377 Screen on Peptide Matrix, PRISMA) (Ramberger et al., 2021) comparing an unmethylated  
378 peptide with a peptide containing an asymmetrically dimethylated arginine. This showed an  
379 impaired interaction of PU.1 with the methylated compared to the unmethylated peptide (**Figure**  
380 **5E**).

381 These results indicate that Carm1 selectively targets arginine 35 of C/EBP $\alpha$  and that the  
382 Carm1-mediated asymmetric dimethylation of this residue decreases the factor's affinity for  
383 PU.1.

384 **Carm1-mediated methylation of arginine 35 modulates C/EBP $\alpha$ -induced BMT**

385 To test the effect of Carm1-mediated methylation of C/EBP $\alpha$  on the factor's ability to induce  
386 BMT, we performed Carm1 gain and loss of function experiments. First, we generated a stable  
387 derivative of the BLaER2 cell line (named RRC3) that contains the reverse tetracycline  
388 transactivator and a doxycycline (Dox)-inducible Carm1 construct. A Western blot confirmed  
389 robust Carm1 expression 24 hours after Dox treatment (**Figure S5D**). Assessing the effects of  
390 Carm1 overexpression on the kinetics of 4-OHT-induced BMT showed a dramatic delay in both  
391 Mac-1 activation and CD19 silencing (**Figure 5F, S6A**). Next, we tested the effect of the Carm1  
392 inhibitor TP064 (Nakayama et al., 2018). After verifying that 5 $\mu$ M of the drug impairs the  
393 asymmetric dimethylation of BAF155 (**Figure S5E**), a known target of Carm1 (Wang et al., 2014)  
394 we found that 4-OHT-induced RRC3 cells treated with 5 $\mu$ M TP064 resulted in a strongly  
395 accelerated BMT (**Figures 5G, S6B**). In contrast, and importantly, C/EBP $\alpha$ <sup>R35A</sup>-mediated BMT  
396 was not delayed by Carm1 overexpression (**Figures S5F, S6C**) nor did the Carm1 inhibitor cause  
397 an acceleration (**Figures S5G, S6D, E**).

398 Our results therefore indicate that high Carm1 expression levels cause a delay in the  
399 kinetics of C/EBP $\alpha$ -induced BMT by methylating R35 of the wild type protein, in line with the  
400 findings obtained with C/EBP $\alpha$  mutant.

401 **Differences of endogenous Carm1 expression correlate with the speed of BMT induction**

402 To investigate the effect of naturally occurring differences in Carm1 expression on BMT  
403 velocity, we used a previously generated single-cell gene expression dataset of cells undergoing  
404 BMT (Francesconi et al., 2019). For this, we monitored Carm1 expression during the BMT  
405 trajectory of single cells by following their similarity to either B cells or macrophages. This showed  
406 that cells with the lowest Carm1 levels were faster in acquiring a macrophage-like identity than  
407 cells with higher levels (**Figure 5H**). The differences leveled off between 42 and 66 hpi,  
408 suggesting that the largest differences occur in the early stages of BMT, in line with the  
409 observation that the kinetics of altered gene expression induced by C/EBP $\alpha$ <sup>WT</sup> and C/EBP $\alpha$ <sup>R35A</sup>  
410 differ mostly at the beginning of the process (**Figure 1F**). These results further support the notion  
411 that Carm1-mediated methylation of arginine 35 modulates the velocity of C/EBP $\alpha$ -induced BMT.

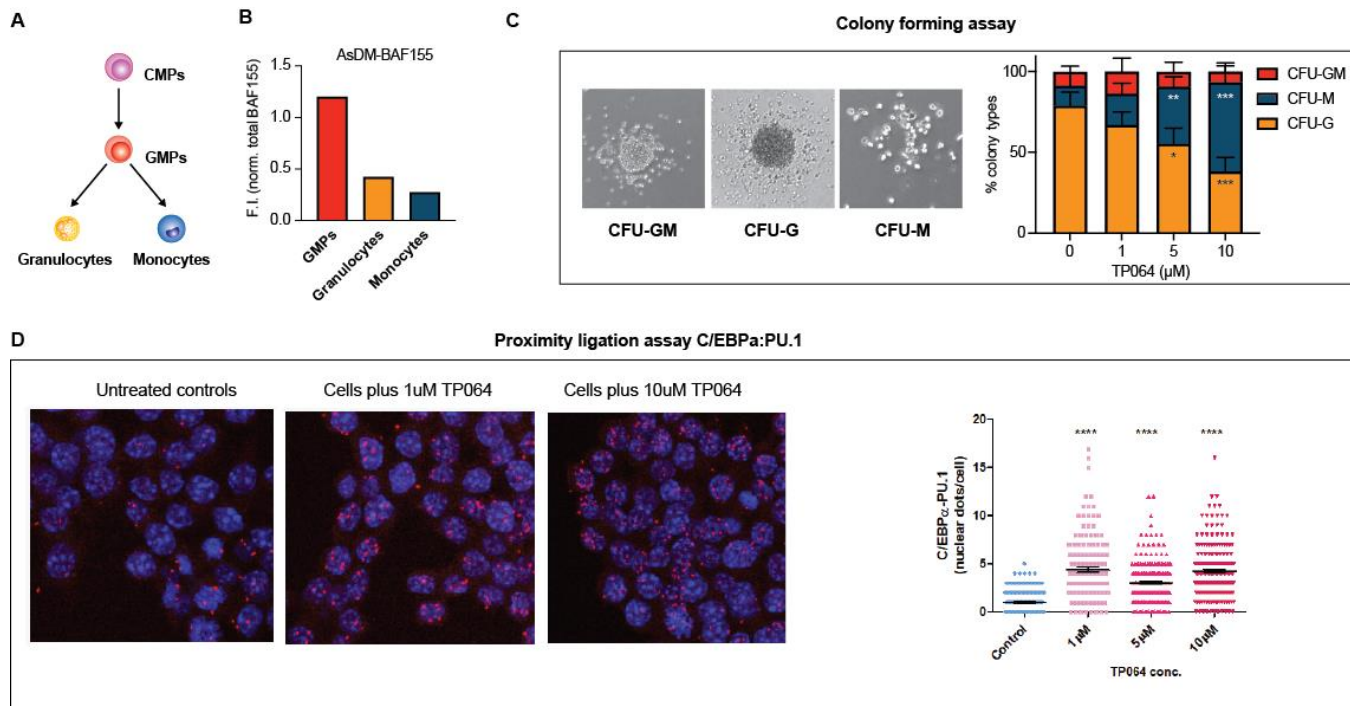
412 **Carm1 inhibition biases GMPs to differentiate towards macrophages**

413 To assess the potential of Carm1 to regulate cell fate decisions during normal myelopoiesis  
414 (**Figure 6A**), we investigated Carm1 RNA expression levels in different myeloid precursors as  
415 well as granulocytes and macrophages, using a dataset obtained earlier (Choi et al., 2019). This  
416 revealed a gradual decrease of Carm1 during the transition from common myeloid progenitors  
417 (CMPs) over GMPs to monocytes and granulocytes (**Figure S7A**). Next, we monitored the levels  
418 of AsDM-BAF155 as a proxy for Carm1 activity in sorted GMPs, granulocytes and monocytes  
419 relative to total BAF155. We observed the highest relative levels of AsDM-BAF155 in GMPs and  
420 a 3.5- and 4.5-fold reduction in granulocytes and monocytes, respectively (**Figure 6B, Figure**  
421 **S7B**). These results suggest that Carm1 RNA levels and enzymatic activity decrease during  
422 myeloid differentiation, reaching their lowest levels at in monocyte/macrophages.

423 To determine whether Carm1 activity affects the decision of GMPs to differentiate into either  
424 granulocytes or monocytes, we tested the effect of the Carm1 inhibitor TP064 in a colony assay.  
425 For this, we isolated GMPs from mouse bone marrow and seeded them in a semisolid medium  
426 containing IL-3 and IL-6 in the presence of 0, 1, 2.5 or 10 $\mu$ M TP064. Scoring the number of the  
427 different myeloid colony types 12 days later showed a dose-dependent reduction of granulocytic  
428 colonies (CFU-G;  $p=0.001$ ) and a concomitant increase of monocytic colonies (CFU-M;  
429  $p=0.0003$ ), with no effect on mixed colonies (CFU-GM;  $p=0.506$ ) (**Figure 6C**). This bias is unlikely

430 due to a granulocyte-selective cytotoxicity of the inhibitor since the total number of colonies  
431 remained essentially constant (**Figure S7C**).

432



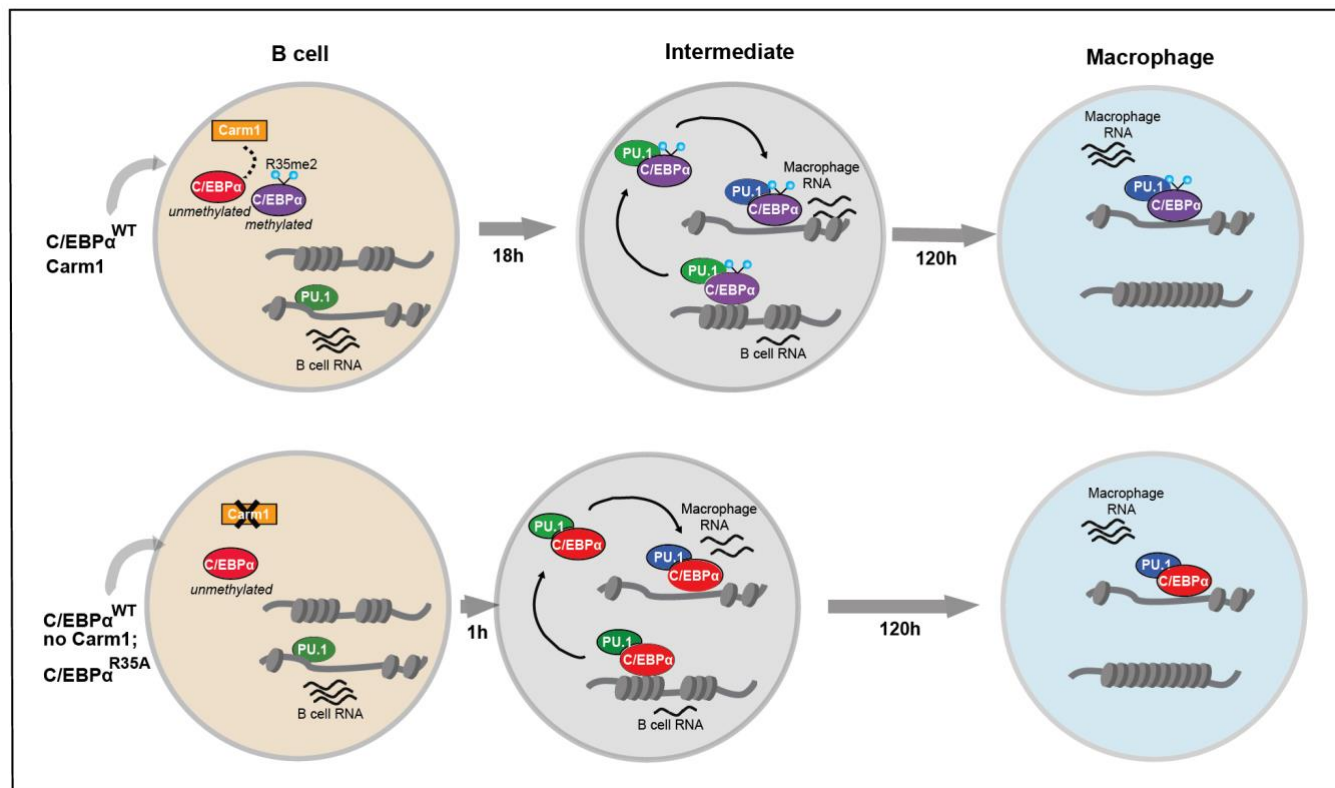
433

434 **Figure 6. Effect of Carm1 activity on myeloid differentiation and C/EBP $\alpha$ -PU.1 interaction.** **A.** Simplified  
435 representation of myeloid differentiation. Common myeloid progenitors (CMPs); granulocyte-macrophage  
436 progenitors (GMPs). **B.** Levels of asymmetrically dimethylated BAF155 (AsDM-BAF155) relative to total BAF155 in  
437 GMPs, granulocytes and monocytes as a proxy for Carm1 activity (see also **Figure S7B**). **C.** On the left,  
438 representative images of colony types obtained from GMPs grown in Methocult. On the right, quantification of colony  
439 numbers obtained in cultures without or with various concentrations of the Carm1 inhibitor TP064 for 14 days,  
440 showing percentage of bipotent (CFU-GM), monocytic (CFU-M) and granulocytic (CFU-G) colonies (mean  $\pm$  s.d.,  
441 n=3-4, statistical significance was determined using a one-way ANOVA for each cell type) (See also **Figure S7C**).  
442 **D.** Proximity ligation assay of endogenous C/EBP $\alpha$  and PU.1 in the mouse macrophage cell line RAW 264.7 treated  
443 for 24 hours with 1, 5 or 10 μM TP064 or left untreated. On the left confocal microscopy images. On the right, counts  
444 of nuclear dots per cell (mean  $\pm$  s.e., n=149-190 cells per condition). Four stars: P<0.0001 (statistical significance  
445 determined using an unpaired Student's t-test.).

446 Together, our results suggest that Carm1 modulates the directionality of GMPs, with  
447 unmethylated C/EBP $\alpha$  biasing them to differentiate towards the monocytic lineage and implying  
448 a role of methylated C/EBP $\alpha$  for the granulocytic lineage.

449 **Carm1 inhibition increases interaction between endogenous C/EBP $\alpha$  and PU.1**

450 The experiments described so far, showing an increased affinity between C/EBP $\alpha$  with a  
451 mutated or an unmethylated R35 and PU.1, were performed after C/EBP $\alpha$  overexpression. To  
452 determine whether an increase in affinity can also be observed between endogenous C/EBP $\alpha$   
453 and PU.1 we tested the effect of Carm1 inhibition on the mouse macrophage line RAW 264.7  
454 (Raschke et al., 1978). For this, the cells were cultured either in the absence or in presence of  
455 1,5 or 10uM of TP064 and subjected to a PLA assay. We observed low numbers of nuclear dots  
456 in the untreated cells and a 4 to 5 fold increase in both cultures treated with the inhibitor (**Figure**  
457 **6D**). This increase was not due to elevated levels of the two proteins in the presence of the  
458 inhibitor, as shown by similar immunofluorescence intensities of C/EBP $\alpha$  and PU.1 (**Figure S7D**).  
459 We conclude that Carm1 inhibition increases the interaction between endogenous C/EBP $\alpha$  and  
460 PU.1, using a macrophage line that expresses similar levels of the two proteins.



461

462 **Figure 7. Proposed mechanism of how Carm1 modulates the velocity of BMT.** The diagram shows the  
463 differences in velocity between a BMT induced by methylated and unmethylated forms of C/EBP $\alpha$ . In condition 1,  
464 cells are induced with C/EBP $\alpha$ <sup>WT</sup> in the presence of Carm1 (upper part). In condition 2 (lower part) cells are induced  
465 with either C/EBP $\alpha$ <sup>WT</sup> in the absence of Carm1 or with C/EBP $\alpha$ <sup>R35A</sup>. Note the more rapid conversion into an  
466 intermediate in the second condition. We hypothesize that C/EBP $\alpha$  induces gene silencing by transiently binding to  
467 gene regulatory elements (GREs) of B cells occupied by PU.1 and other B cell transcription factors. This leads to

468 the release of the C/EBP $\alpha$ :PU.1 complex (and probably the other B cell factors) and chromatin closing. C/EBP $\alpha$ :PU.1  
469 complexes then relocate to myeloid GREs, where they induce chromatin opening and activation of macrophage  
470 gene expression. Carm1-mediated methylation of arginine 35 delays the BMT by impairing the interaction of C/EBP $\alpha$   
471 with PU.1 and relocation of PU.1 to myeloid GREs. The green symbol for PU.1 implies its role as a B cell regulator,  
472 blue as a myeloid regulator.

## 473 **DISCUSSION**

474 Here we describe a mechanism by which the speed of a hematopoietic cell fate decision is  
475 modulated. Using a model system in which C/EBP $\alpha$  induces a B cell to macrophage  
476 transdifferentiation (BMT) we found that an arginine 35 mutant dramatically accelerates the  
477 process. As summarized in Figure 7, our data, together with that of earlier work (van Oevelen et  
478 al., 2015) suggest that C/EBP $\alpha$  initiates B cell gene silencing by binding to specific GREs, a  
479 subset of which occupied by PU.1 in addition to B cell restricted regulatory factors. This binding  
480 is transient and leads to the rapid release of the complex from chromatin by an unknown  
481 mechanism. The free C/EBP $\alpha$ -PU.1 complex in turn translocates to macrophage-specific GREs,  
482 inducing chromatin opening and the activation of myeloid genes. During this relocation, PU.1  
483 essentially switches from a B cell regulator to a myeloid regulator, now binding to a set of largely  
484 myeloid-specific GREs. The speed of this conversion is regulated by the levels of Carm1 in the  
485 starting cell, which determines the proportion of methylated or unmethylated arginine C/EBP $\alpha$  at  
486 R35. In this stealing model the C/EBP $\alpha^{R35A}$  mimics the unmethylated form of the factor, showing  
487 a stronger affinity for PU.1 than wild type C/EBP $\alpha$ . The model however, does not explain how  
488 PU.1 becomes removed from B cell GREs that are not detectably bound by C/EBP $\alpha$ .

489 The observed near symmetrical acceleration of activation and silencing of B cell and  
490 myeloid-restricted genes induced by C/EBP $\alpha^{R35A}$  or by C/EBP $\alpha^{WT}$  in cells with reduced Carm1  
491 activity suggests that PU.1 acts as a cell fate coordinator, preventing the formation of cells with  
492 aberrantly regulated lineage programs. Whether during the C/EBP $\alpha$ -induced BMT PU.1 acquires  
493 a different conformation when it turns from a B cell to a myeloid regulator will be interesting to  
494 determine. A critical parameter for the enhancement of myeloid differentiation during the  
495 conversion of a fetal liver T cell precursor into macrophages has been described to be cell cycle  
496 length, with cell cycle extension leading to the accumulation of high PU.1 levels (Kueh et al.,  
497 2013). Whether under physiological conditions this lengthening is induced by the activation of

498 endogenous C/EBP $\alpha$ , itself known to be a potent inhibitor of the cell cycle (Nerlov, 2007), and  
499 whether it is exacerbated by a mutation of R35 remains to be studied.

500 A transcription factor stealing mechanism has also been described for T cell differentiation.  
501 Thus, at the DN1 progenitor stage PU.1 forms a complex with Satb1 and Runx1 at GREs of  
502 PU.1-dependent genes. Once PU.1 becomes downregulated at the DN3 stage, the associated  
503 factors are released and relocate to T cell GREs where they upregulate T cell genes (Hosokawa  
504 et al., 2018). However, in contrast to the mechanism described here, where C/EBP $\alpha$  acts as the  
505 ‘thief’ and PU.1 as the ‘victim’, PU.1 is the ‘thief’. In another relevant example T-bet relocates  
506 Gata3 from T<sub>H</sub>2 to T<sub>H</sub>1 genes during TH1 specification (Hertweck et al., 2022). These studies  
507 support the notion that transcription factor ‘stealing’ could be a more general mechanism by  
508 which cells coordinate silencing of the old and activation of the new differentiation program.

509 Remarkably, C/EBP $\alpha^{R35A}$  expression in B cells generates a myeloid cell-like state already  
510 within 1 hpi, only seen with the wild type after 18 hpi. Whether the observed catching up in gene  
511 expression after 120 h in C/EBP $\alpha^{WT}$ - induced cells occurs gradually or in a more narrowly defined  
512 time window remains to be determined. Reflecting these observations, the capacity of C/EBP $\alpha$   
513 to induce a transition of closed to open chromatin in fibroblasts is remarkably fast compared to  
514 other pioneer transcription factors (Lerner et al., 2020). That co-expression of PU.1 further  
515 accelerates chromatin opening in fibroblasts while activating the myeloid program suggests a  
516 powerful synergism between the two pioneer factors, regulated by methylation of arginine 35.  
517 BMT completion requires 3 to 5 days for mouse cells while human cells require 5 to 7 days  
518 (Rapino et al., 2013; Xie et al., 2004), raising the possibility that species-specific differences in  
519 Carm1 activity play a role. However, the observation that inhibition of Carm1 accelerates BMT  
520 not only in human but also in mouse cells makes this unlikely. It will be interesting to determine  
521 whether the observed species differences of BMT length reflects a higher protein stability in the  
522 human cells, as reported for neuronal specification (Rayon et al., 2020), although other  
523 mechanisms have also been described (Ebisuya and Briscoe, 2018).

524 In line with the results described here that Carm1 inhibition biases GMPs to differentiate into  
525 macrophage colonies, HSCs lacking Carm1 have been shown to be biased towards monocyte  
526 formation (Greenblatt et al., 2018). These observations suggest that methylated C/EBP $\alpha$  is  
527 required for the decision of GMPs to become granulocytes, and that this form of the factor is not

528 simply inactivated during macrophage specification. A role of transcription factor methylation by  
529 Carm1 has also been described for muscle differentiation. Here, asymmetric dimethylation of  
530 four arginines in Pax7 enables recruitment of the MLL complex. As a consequence, Myf5  
531 becomes transcriptionally activated, resulting in muscle cell specification (Chang et al., 2018;  
532 Kawabe et al., 2012). Carm1 has also been implicated in early embryo development and several  
533 targets have been described, including histones and chromatin modifying factors (Suresh et al.,  
534 2021; M.-E. Torres-Padilla et al., 2007), but whether this also involves the methylation of a key  
535 transcription factor is unknown.

536 Our observations challenge the notion that binary cell fate decisions simply result from the  
537 relative expression of antagonistic transcription factors (Graf and Enver, 2009; Moris et al., 2016).  
538 Rather, post-translational modifications, such as described here, may act as an additional  
539 regulatory layer (Torcal Garcia and Graf, 2021). Thus, the proportions of a modified versus  
540 unmodified transcription factor within a precursor population could be subject to external  
541 signaling that activates Carm1 or another enzyme that induces posttranslational modifications.  
542 Such a mechanism could operate regardless of whether binary cell fate decisions occur gradually  
543 as reported for hematopoiesis (Velten et al., 2017) or abruptly as during a neuronal differentiation  
544 cascade (Konstantinides et al., 2022). How the timing of alternative cell fate decisions is  
545 regulated is relevant not only for a better understanding of cell differentiation but also for  
546 aberrations in developmental diseases such as certain types of cancer.

547

## 548 ACKNOWLEDGEMENTS

549 We thank the T.G. laboratory members for critical discussions, the Flow Cytometry and  
550 Microscopy units of UPF-CRG for technical assistance, the CRG Genomics core facility for  
551 sequencing and Lars Velten for feedback on the manuscript. Work in the laboratory of T. G. was  
552 supported by the Spanish Ministry of Economy, Industry and Competitiveness, (Plan Estatal  
553 PID2019-109354GB-100), the CRG, AGAUR (SGR 726) and a European Research Council  
554 Synergy grant (4D-Genome). Work in the laboratory of K.S.Z. was supported by NIH  
555 (R01GM36477).

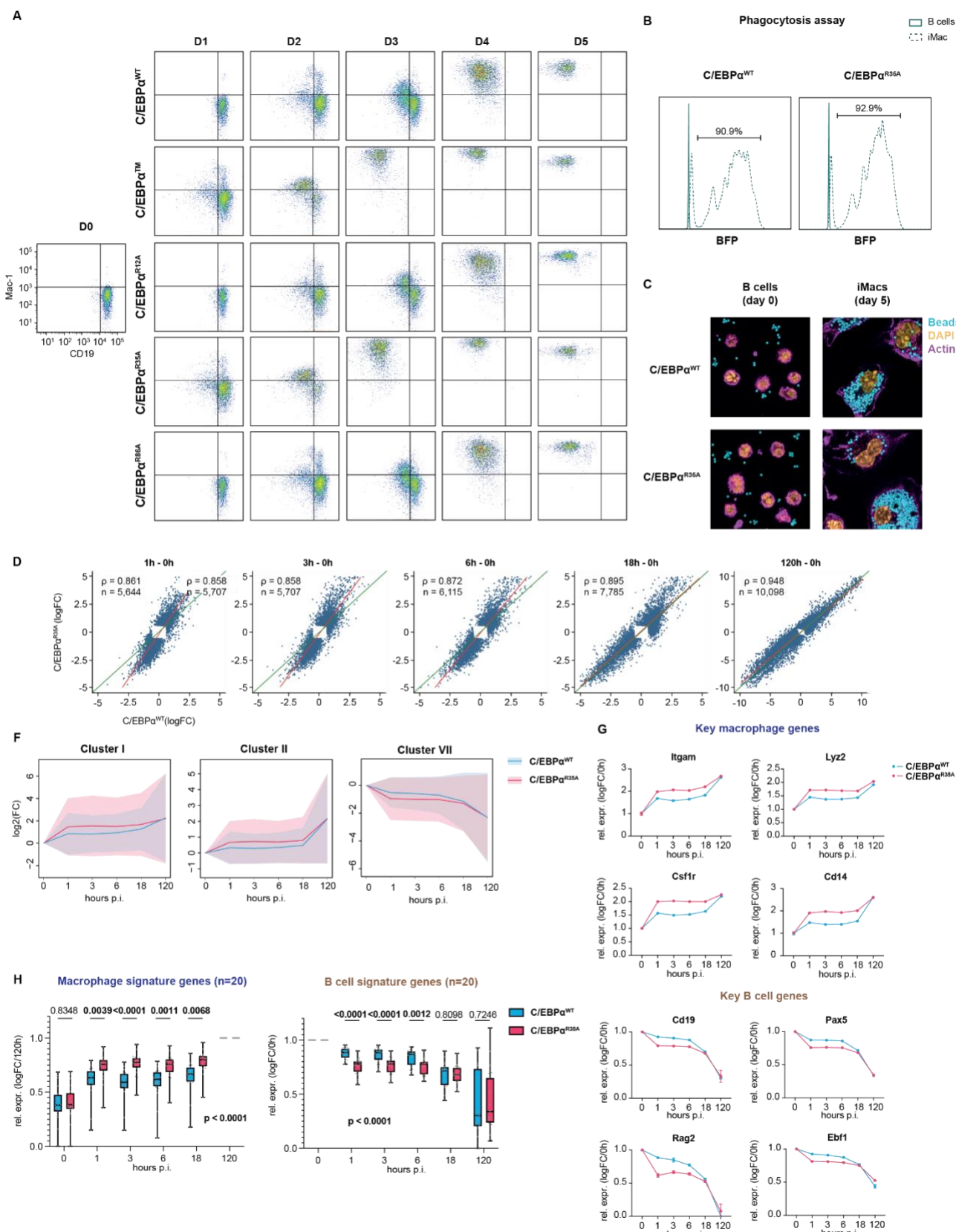
556 **AUTHOR CONTRIBUTIONS**

557 G.T.G and T.G. conceived the study and wrote the manuscript. G.T.G. performed  
558 transdifferentiation experiments (BMT and fibroblasts), cell line generation, RNA- and ATAC-seq,  
559 plasmid construction, immunofluorescence, and data analyses. E.K-L performed co-  
560 immunoprecipitation, EMSA and *in vitro* methylation assays. T.V.T. performed BMT, RNA- and  
561 ATAC-seq. A.K. and M.V-C. processed RNA-, ATAC- and ChIP-seq data. J.L. performed SMT  
562 experiments. L.A-A. performed co-immunoprecipitation, FACS, PLA and colony assays. C.B-B.  
563 performed BMT. M.P-C. confocal microscopy. R.B. and M.F. analyzed single cell expression  
564 data. S.P., K.Z., A.L. contributed ideas and discussions.

565

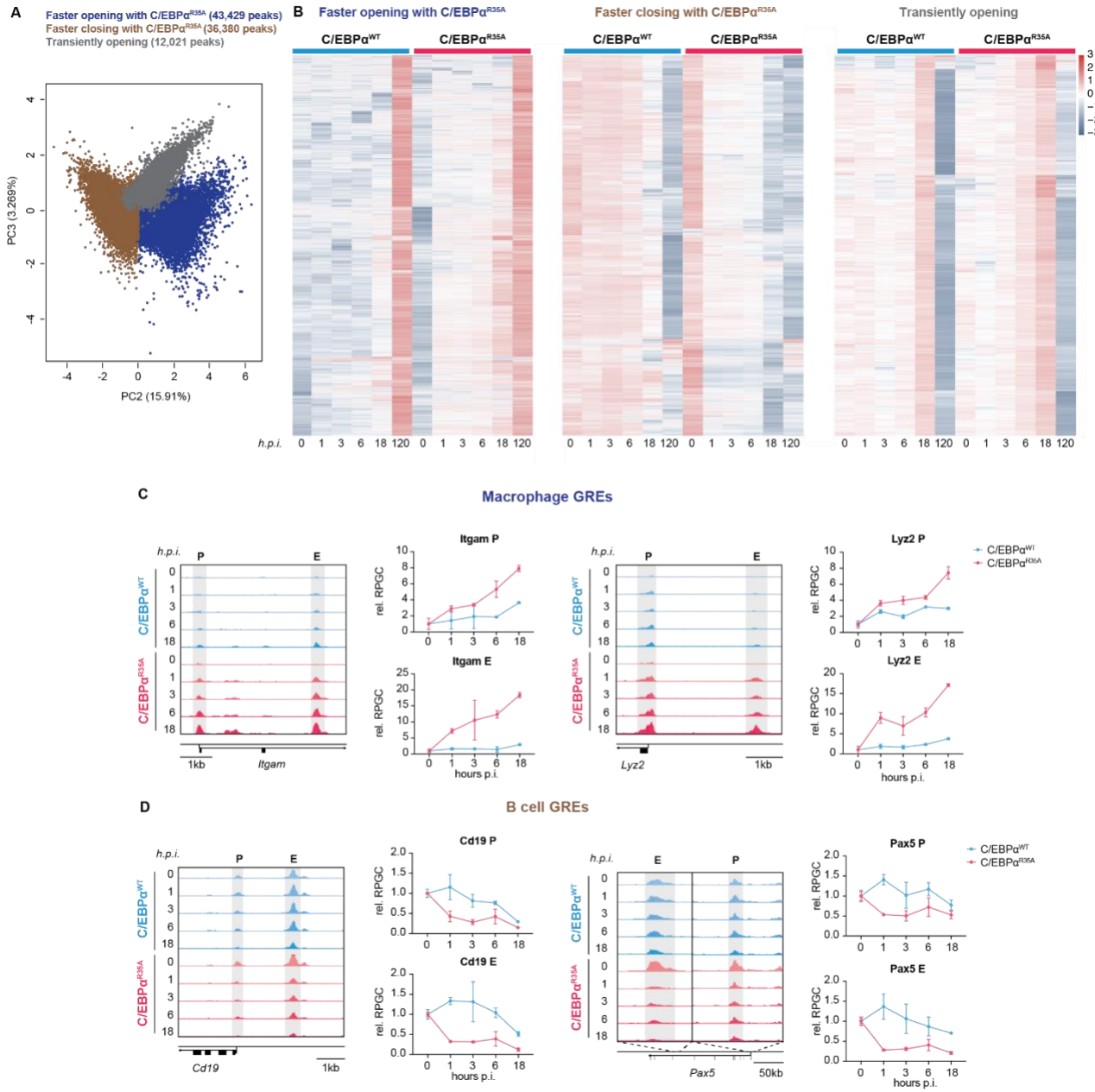
566

567 **SUPPLEMENTAL INFORMATION**



569 **Figure S1. Mutation of arginine 35 in C/EBP $\alpha$  accelerates B cell gene silencing and macrophage gene  
570 activation. Related to Figure 1.** **A.** FACS plots of Mac-1 (CD11b) and CD19 expression in B cells induced with  
571 C/EBP $\alpha$ <sup>WT</sup>, C/EBP $\alpha$ <sup>TM</sup>, C/EBP $\alpha$ <sup>R12A</sup>, C/EBP $\alpha$ <sup>R35A</sup> or C/EBP $\alpha$ <sup>R86A</sup> at different days p.i. **B.** Histograms showing  
572 fluorescence intensity of internalized BFP carboxylated beads in C/EBP $\alpha$ <sup>WT</sup> and C/EBP $\alpha$ <sup>R35A</sup>-induced cells (dashed  
573 line) incubated overnight by flow cytometry. Data for uninduced control B cells are represented by a continuous line.  
574 Percentage of phagocytic cells is indicated. **C.** Immunofluorescent images of uninduced (day 0) and 5 days-induced  
575 pre B cells incubated overnight with BFP carboxylated beads. DNA was stained with picogreen (P7589) and F-actin  
576 with phalloidin Alexa Fluor 568. **D.** Scatter plots showing gene expression changes at 1, 3, 6, 18 and 120 hpi relative  
577 to 0h for B cells induced with either C/EBP $\alpha$ <sup>WT</sup> or C/EBP $\alpha$ <sup>R35A</sup>. Red line = regression line fitted to each scatter plot;  
578 green line = identity line ( $x=y$ );  $\rho$  = Spearman correlation coefficient;  $n$  = number of differentially expressed genes.  
579 **E.** Kinetics of gene expression of clusters I, II and VII of B cells induced with either C/EBP $\alpha$ <sup>WT</sup> (cyan) or C/EBP $\alpha$ <sup>R35A</sup>  
580 (magenta) at different times p.i. The Y axis shows log2 fold-changes relative to uninduced cells. The lines and the  
581 shaded backgrounds correspond to the mean  $\pm$  1.64 s.d.,  $n=1103-1868$ . **F.** RNA expression levels of key  
582 macrophage or B cell genes in B cells induced by either C/EBP $\alpha$ <sup>WT</sup> (cyan) or C/EBP $\alpha$ <sup>R35A</sup> (magenta) relative to 0h  
583 (mean  $\pm$  s.d.,  $n=2$ ). **G.** RNA expression levels of selected macrophage and B cell signature genes in B cells induced  
584 by either C/EBP $\alpha$ <sup>WT</sup> (cyan) or C/EBP $\alpha$ <sup>R35A</sup> (magenta) relative to 120h and 0h, respectively (median and quartiles are  
585 represented,  $n=20$ , statistical significance was determined using multiple paired Student's t-test for individual  
586 timepoint comparisons as well as Two-way ANOVA for overall statistical significance).

587

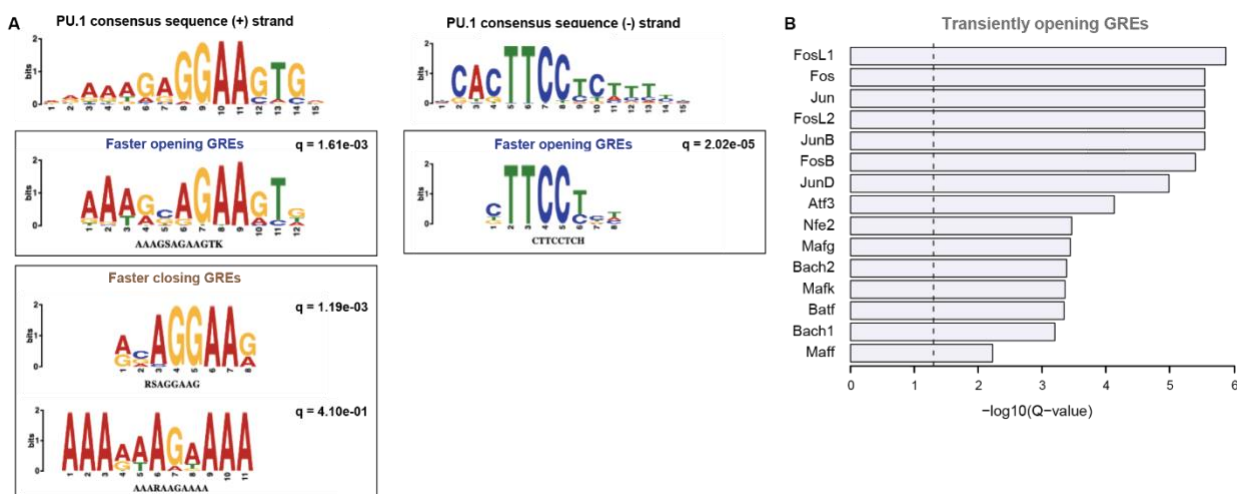


588

589 **Figure S2.  $C/EBP\alpha^{R35A}$  accelerates chromatin remodeling at regulatory elements of lineage-restricted genes.**  
 590 **Related to Figure 2. A.** PCA analysis of individual peaks showing PC2 and PC3 and the three clusters that were  
 591 generated ( $n = 91,830$  peaks). **B** Three clusters were generated from a PCA analysis shown in A. The clusters show  
 592 three main trends: regions that are opened throughout BMT, more rapidly so with  $C/EBP\alpha^{R35A}$  (blue); regions that  
 593 are closed throughout BMT, also more rapidly so with  $C/EBP\alpha^{R35A}$  (brown); and regions that peak at 18h and are  
 594 closed at 120h (grey). **C.** Gene ontology (GO) enrichment of macrophage-myeloid and B cell terms of each cluster  
 595 from Figure 2C. Diameter of circles is proportional to the p-value. Colored circles indicate significant enrichment.  
 596 Chromatin accessibility kinetics of key macrophage (**D**) and B cell (**E**) gene regulatory elements (GREs). Genome  
 597 browser views of ATAC peaks (gray highlight; P=promoter, E=enhancer) corresponding to known or putative GREs

598 of macrophage (*Itgam* and *Lyz2*) and B cell genes (*Cd19* and *Pax5*). Genes, direction of transcription and scale are  
599 indicated in each panel. Kinetics of chromatin accessibility at different timepoints are displayed for C/EBP $\alpha$ <sup>WT</sup> (cyan)  
600 and C/EBP $\alpha$ <sup>R35A</sup> (magenta) as reads per genomic content relative to 0h (RPGC).

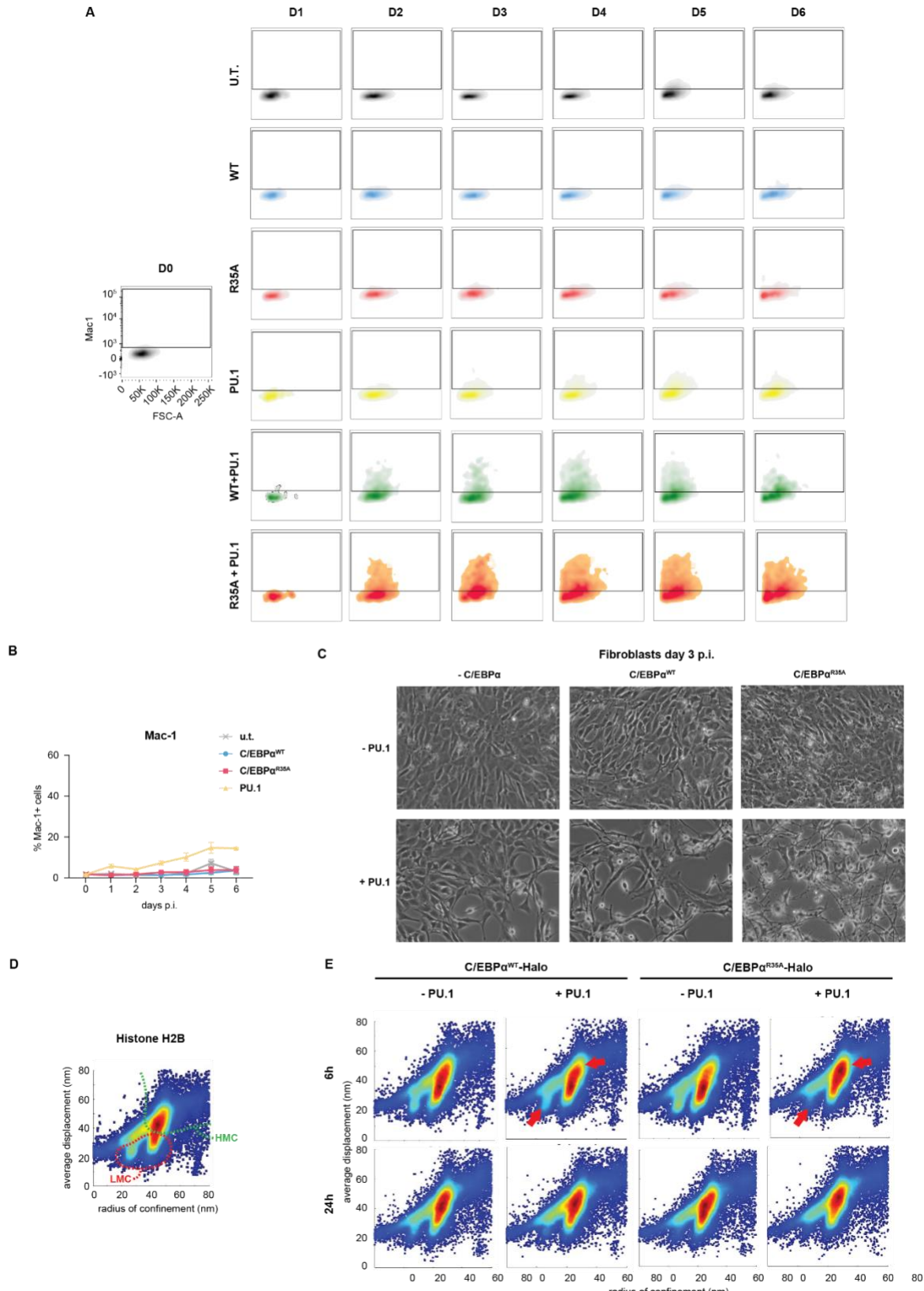
601



602

603 **Figure S3. C/EBP $\alpha^{R35A}$  selectively interacts with PU.1. Related to Figure 3. A.** PU.1 enriched motifs related to  
604 Figure 3D. PU.1 consensus sequence in the + and – strand is displayed (top), as well as matched enriched de novo  
605 motifs. **B.** De novo motifs matched to known TF motifs in putative in GRES that are transiently opened (grey)  
606 obtained in Figure S2A and B. Top 20 motifs are ordered by significance.

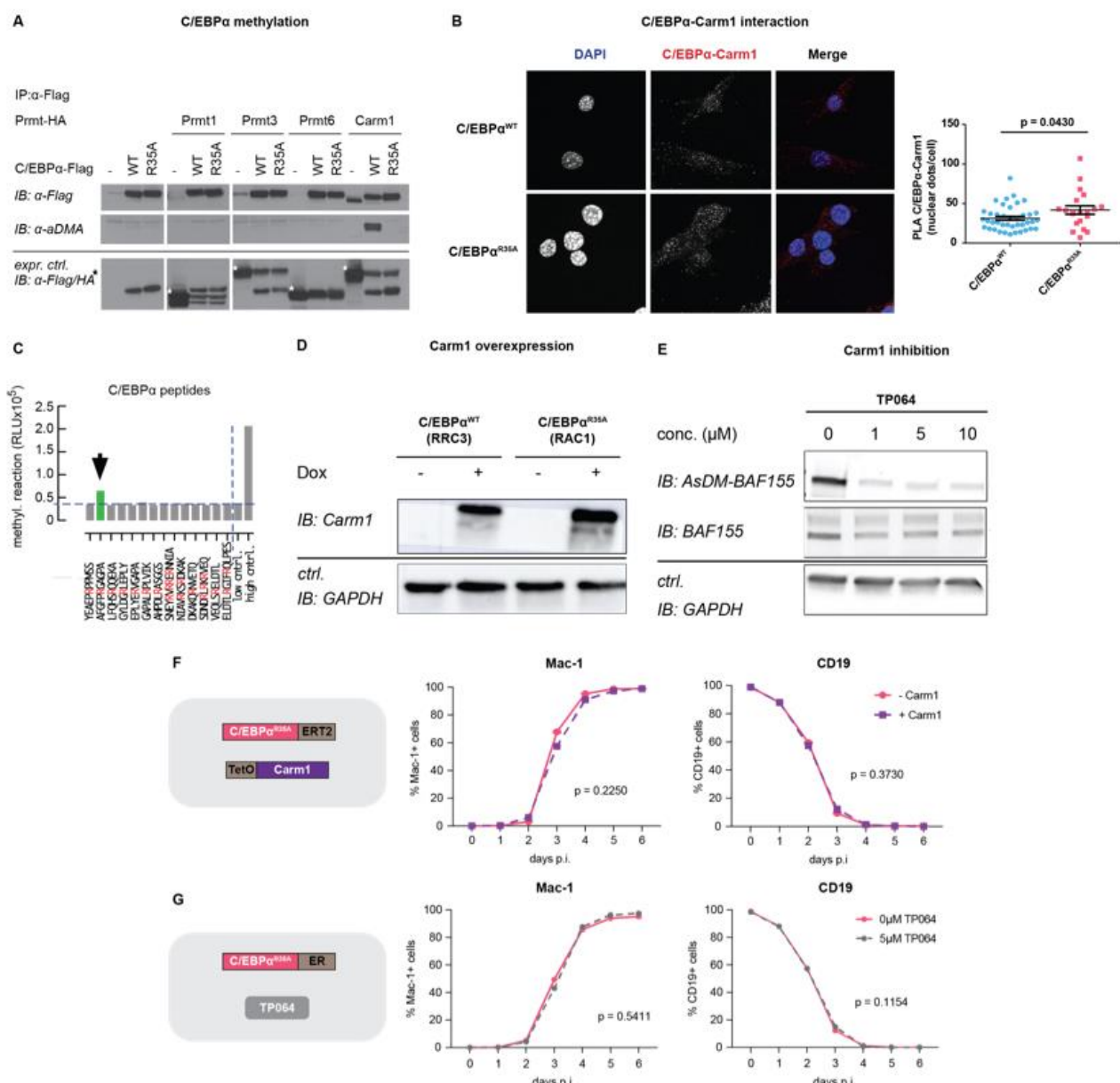
607



608

609 **Figure S4. C/EBPα<sup>R35A</sup> hastens the relocation of PU.1 from B cell to myeloid GREs. Related to Figure 4. A.**

610 FACS plots of the fibroblast to macrophage transdifferentiation by co-expression of either C/EBP $\alpha$ <sup>WT</sup> or C/EBP $\alpha$ <sup>R35A</sup>  
611 and PU.1 measured by Mac-1 expression by flow cytometry. **B.** Kinetics of macrophage transdifferentiation induced  
612 by C/EBP $\alpha$ <sup>WT</sup>, C/EBP $\alpha$ <sup>R35A</sup> or PU.1 and untransduced cells (u.t.) measured by Mac-1 expression by FACS (mean  $\pm$   
613 s.d., n=3, statistical significance was determined using two-way ANOVA). **C.** Phase contrast images of NIH3T3 cells  
614 induced with either C/EBP $\alpha$ <sup>WT</sup> or C/EBP $\alpha$ <sup>R35A</sup> and PU.1 in different combinations for 3 days. **D.** Single molecule-  
615 tracking (SMT) of histone H2B in 3T3 cells transfected with an H2B-Halo tag construct for 24h (n = 20,000). Average  
616 displacement and radius of confinement are displayed, and chromatin mobility groups were identified (vL = very low;  
617 L = low; I = intermediate; H = high). **E.** Single molecule-tracking (SMT) of either C/EBP $\alpha$ <sup>WT</sup> or C/EBP $\alpha$ <sup>R35A</sup> in 3T3  
618 cells infected with a Dox-inducible C/EBP $\alpha$ -Halo constructs for either 6 or 24h with or without PU.1 co-expression  
619 (n = 20,000).

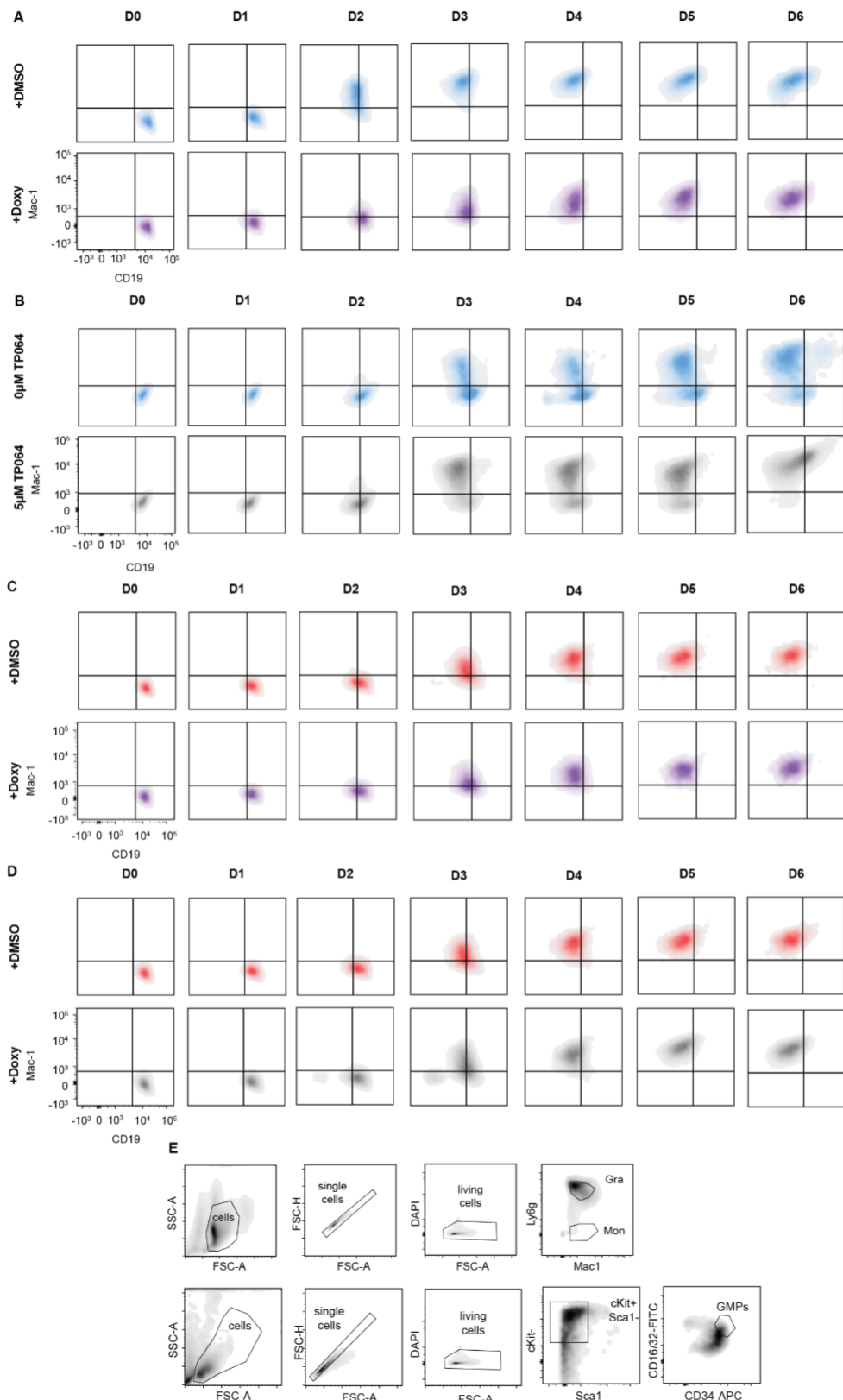


620

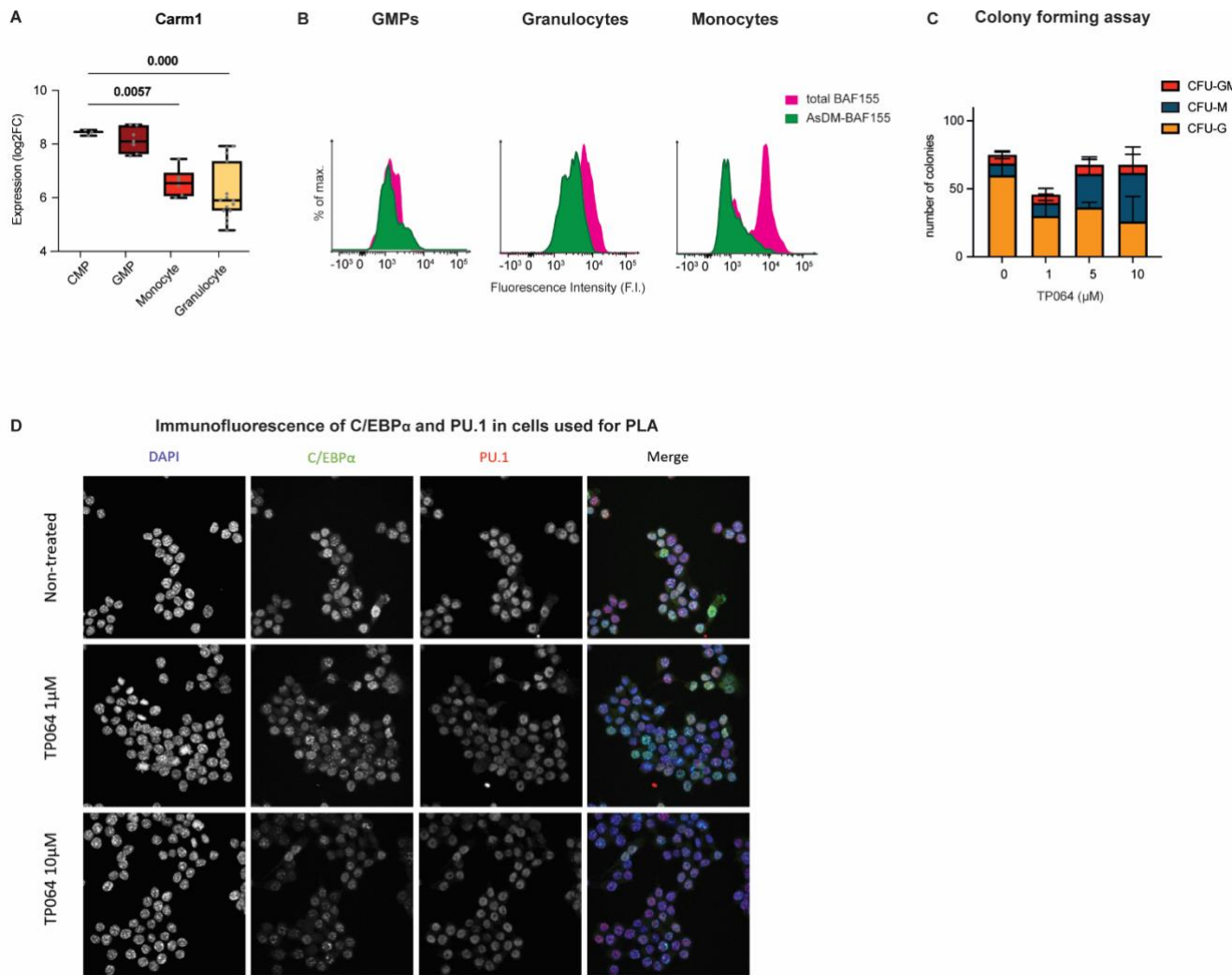
621 **Figure S5. Carm1-mediated methylation of arginine 35 regulates interaction between the two proteins and**  
 622 **the speed of C/EBP $\alpha$ -induced BMT. Related to Figure 5. A.** Immunoprecipitation of C/EBP $\alpha$ <sup>WT</sup> or C/EBP $\alpha$ <sup>R35A</sup>  
 623 (Flag) from HEK293-T cells co-transfected with either C/EBP $\alpha$ <sup>WT</sup>- or C/EBP $\alpha$ <sup>R35A</sup>-Flag and different type I Prmt  
 624 enzymes (Prmt1, Prmt3, Prmt6 and Carm1), followed by immunoblot with antibodies against asymmetrically  
 625 dimethylated arginine (aDMA), Flag or HA. **B.** Proximity ligation assay of Carm1 and C/EBP $\alpha$ <sup>WT</sup> or C/EBP $\alpha$ <sup>R35A</sup> in  
 626 fibroblast lines 3T3aER-R and 3T3aER-A, respectively, induced with  $\beta$ -estradiol for 24 hours. On the left, images of  
 627 the cells showing DNA stained with DAPI and interaction between C/EBP $\alpha$  and Carm1. On the right, quantification  
 628 of interaction by nuclear dots per cell (mean  $\pm$  s.e.; n=20-40, statistical significance was determined using an  
 629 unpaired Student's t-test). **C.** In vitro methylation assay using Carm1 and 13 arginine-containing peptides spanning  
 630 the entire C/EBP $\alpha$  protein (15 peptides, 20 R-residues highlighted in red). Peptide containing R35 bar indicated in

631 green. Low control: no enzyme; high control: optimized R-methylation peptide, provided by BPS Bioscience) **D**.  
632 Western blot of Carm1 in B cell lines RRC3 and RAC1 with or without addition of Dox. **E**. Western blot of  
633 asymmetrically dimethylated BAF155 (AsDM-BAF155) and total BAF155 (BAF155) in B cells treated with different  
634 concentrations of TP064 (1-10 $\mu$ M). **F**. Kinetics of C/EBP $\alpha$ <sup>R35A</sup>-mediated BMT upon Carm1 overexpression by pre-  
635 treatment with Dox for 24h measured by Mac-1 and CD19 expression by flow cytometry (mean  $\pm$  s.d.; n=3, statistical  
636 significance was determined using two-way ANOVA). **G**. Kinetics of C/EBP $\alpha$ <sup>R35A</sup>-mediated BMT upon Carm1  
637 inhibition by pre-treatment with TP064 for 24h measured by Mac-1 and CD19 expression by flow cytometry (mean  
638  $\pm$  s.d.; n=3, statistical significance was determined using two-way ANOVA).

639



642 **to Figure 5. A.** FACS plots showing BMT of cells induced with C/EBP $\alpha$ <sup>WT</sup> and exposed to Carm1 overexpression  
643 after staining for the lineage markers Mac-1 and CD19. **B.** FACS plots showing BMT of cells induced with C/EBP $\alpha$ <sup>WT</sup>  
644 and exposed to 5 $\mu$ M TP064 after staining for the lineage markers Mac-1 and CD19. **C.** FACS plots showing BMT of  
645 cells induced with C/EBP $\alpha$ <sup>R35A</sup> and exposed to Carm1 overexpression after staining for the lineage markers Mac-1  
646 and CD19. **D** FACS plots showing BMT of induced with C/EBP $\alpha$ <sup>R35A</sup> and exposed to 5 $\mu$ M TP064 after staining for  
647 the lineage markers Mac-1 and CD19. **E.** Gating strategy for sorting of bone marrow-derived granulocytes,  
648 monocytes (upper panels) and GMPs (lower panels).



649 **Figure S7. Dimethylation of C/EBP $\alpha$  by Carm1 is involved in the lineage choice of hematopoietic cells and**  
650 **C/EBP $\alpha$ :PU.1 interaction. Related to Figure 6 A.** Expression of Carm1 during myeloid differentiation obtained  
651 from RNA-seq published data (Choi et al., 2019) (quartiles are represented, n=3-7, statistical significance was  
652 determined using multiple unpaired Student's t-tests). **B.** FACS plots showing levels asymmetrically dimethylated  
653 (AsDM)-BAF155 and total BAF155 in GMPs, granulocytes and monocytes. The histograms represent fluorescence  
654 of each fraction of the protein. **C.** Colony forming unit (CFU) assay of GMPs in various concentrations of the Carm1  
655 inhibitor TP064 after 14 days in Methocult. Total number of bipotent (CFU-GM), monocytic (CFU-M) and granulocytic  
656 (CFU-G) colonies.

657 (CFU-G) colonies are shown (mean  $\pm$  s.d., n=3-4, statistical significance was determined using a one-way ANOVA).  
658 D. C/EBP $\alpha$  and PU.1 fluorescence in RAW cells used for PLA in Figure 6. DNA was stained with DAPI, C/EBP $\alpha$   
659 with AF488 and PU.1 with AF546.

660

661

662 **MATERIALS AND METHODS**

663 **Mice**

664 As a source for the B cells used in our experiments, we used C57BL/6J mice. During experiments  
665 the number of female and male mice was balanced. Mice were housed in standard cages under  
666 12h light-dark cycles and fed *ad libitum* with a standard chow diet. All experiments were approved  
667 by the Ethics Committee of the Barcelona Biomedical Research Park (PRBB) and performed  
668 according to Spanish and European legislation.

669 **Cells and cell cultures**

670 CD19+ B cells were isolated from the bone marrow with a monoclonal antibody to CD19 (BD  
671 Biosciences, Cat#553784) using MACS sorting technology (Miltenyi Biotech) as previously  
672 described (Di Stefano, 2016). Bone marrow-derived B cells were cultured on gelatinized plates  
673 containing S17 feeder cells in RPMI culture medium (GIBCO, Cat#12633012) containing 20%-  
674 FBS (GIBCO, Cat#10270-106), 100 U/mL Penicillin- 100 ng/mL Streptomycin (GIBCO,  
675 Cat#15140122), 2mM L-Glutamine (GIBCO, Cat#25030081) and 0.1mM 2-Mercaptoethanol  
676 (Invitrogen, Cat#31350010)(further addressed as **mouse B cell medium**), which was further  
677 supplemented with 10 ng/mL of IL-7 (Peprotech, Cat#217-17). HEK293-T, NIH3T3 cells (and  
678 derived) and MEFs were cultured in 10% FBS (GIBCO, Cat#10270-106) DMEM (GIBCO,  
679 Cat#12491015) medium. The final culture medium also contained 100U/mL Penicillin and  
680 100ng/mL Streptomycin (GIBCO, Cat#15140122), 2mM L-Glutamine (GIBCO, Cat#25030081)  
681 and 0.1mM 2-Mercaptoethanol (Invitrogen, Cat#31350010) (further addressed as DMEM  
682 complete medium). RCH-ACV (and derived) human B cells were grown in RPMI culture medium  
683 (GIBCO, Cat#22400089) containing 20%-FBS (10270-106, GIBCO) (further addressed as  
684 human B cell medium).

685 **Induction of mouse B cell to macrophage transdifferentiation**

686 Induction of transdifferentiation of primary pre/pro B cells (heretofore referred as B cells) isolated  
687 from the bone marrow of C57BL/6J mice was performed as previously described(Xie et al.,  
688 2004a). Briefly, B cells isolated from 8-16 weeks C57BL/6J mice were infected with C/EBP $\alpha$ -ER-  
689 hCD4 retrovirus, plated at 500 cells/cm<sup>2</sup> in gelatinized plates (12 wells) onto mitomycin-C (Sigma,  
690 Cat#M0503)-treated MEFs (10 $\mu$ g/mL mitomycin-C for 3 hours to inactivate MEFs). Cells were  
691 transdifferentiated in mouse B cell medium, which was further supplemented with 10 ng/mL each

692 of IL-7 (Peprotech, Cat#217-17), IL-3 (Peprotech, Cat#213-13), FLT-3 (Peprotech, Cat#250-31),  
693 mCSF-1 (Peprotech, Cat#315-03B), mSCF (Peprotech, Cat#250-03) and 100 nM  $\beta$ - estradiol  
694 (Merck Millipore, Cat#3301) to shuttle C/EBP $\alpha$  into the cell nucleus. Culture medium was  
695 renewed every 2 days with the same composition but without IL-7.

696 **Induction of fibroblast to macrophage transdifferentiation**

697 Fibroblast transdifferentiation into macrophage experiments were performed as previously  
698 described (Feng et al., 2008b). Briefly, NIH 3T3 fibroblasts were infected with C/EBP $\alpha$ -ER-IRES-  
699 hCD4 retrovirus and hCD4 positive cells were sorted and a cell line was established. Cells were  
700 plated at 200,000 cells/ml in gelatinized 6-well plates and infected with PU.1 $\Delta$ PEST-IRES-GFP  
701 retrovirus. After 24 hours cells were re-plated at 30,000 cells/ml in gelatinized 24-well plates in  
702 DMEM complete medium supplemented with IL-3 (Peprotech, Cat#213-13) mCSF-1 (Peprotech,  
703 Cat#315-03B) and 100 nM  $\beta$ -estradiol (Merck Millipore, Cat#3301) to shuttle C/EBP $\alpha$  into the  
704 nucleus.

705 **Induction of human B cell to macrophage transdifferentiation**

706 Transdifferentiation of human B cells from the B lymphoblastic leukemia cell line RCH-ACV was  
707 performed as previously described (Rapino et al., 2013b). Briefly, RCH-ACV cells were infected  
708 with C/EBP $\alpha$ -ER-IRES-GFP retroviruses and GFP-positive cells were sorted, and clonal lines  
709 (BLaER2 and BLaER2-A) were generated. These lines were then infected with rtTA-Puromycin  
710 retroviruses and selected with 1 $\mu$ g/mL of Puromycin for 1 week. Selected cells were further  
711 infected with pHAGE-TetO-Carm1-IRES-dTomato lentiviruses. Cells were grown in human B cell  
712 medium, supplemented with 2  $\mu$ g/mL of doxycycline (Sigma, Cat#D9891). Tomato-positive cells  
713 were sorted, and clonal cell lines were established (RRC3 and RAC1). For transdifferentiation  
714 cells were grown in human B cell medium, which was further supplemented with 10 ng/mL each  
715 of IL-3 (Peprotech, Cat#200-03), CSF-1 (Peprotech, Cat#315-03B) and 2.5  $\mu$ M 4-  
716 hydroxytamoxifen (4-OHT) (Sigma, Cat#H7904) to shuttle C/EBP $\alpha$  into the cell nucleus.

717 **Hematopoietic colony forming assay**

718 Bone marrow-derived GMPs from C57BL/6J mice were isolated by FACS sorting and cultured in  
719 Methocult GF M3434 (03434, Stem Cell Technologies) for 14 days. Cells were harvested from  
720 the Methocult cultures, and colonies were investigated by microscopy.

721 **Cell transfection**

722 HEKT-293T cells were transfected with C/EBPa WT or mutant expression vectors in the absence or  
723 presence of PRMT1-HA, PRMR3-HA, CARM1-HA, PRMT6-HA or Pu.1 as indicated using  
724 Polyethylenimine according to the manufacturer's protocol (PEI, Polysciences, Cat#24765-2)

725 **Lentivirus production and infection**

726 Lentiviruses were produced by transfecting HEK-293T cells with 6 $\mu$ g of pCMV-VSV-G, 15 $\mu$ g of  
727 pCMVDR-8.91, and 20 $\mu$ g of the lentiviral vector using the calcium phosphate transfection  
728 method. Briefly, calcium phosphate-DNA precipitates were prepared by pooling the upper  
729 amounts of the three plasmids in a 2.5M CaCl<sub>2</sub> aqueous solution. While vortexing, one volume  
730 of HBS 2X (HEPES-buffered saline solution pH=7.05, 280mM NaCl, 0.05M HEPES and 1.5mM  
731 Na<sub>2</sub>HPO<sub>4</sub>) was added dropwise to an equal volume of the calcium phosphate-DNA solution.

732 The mixture was incubated for 15 minutes at room temperature and added dropwise to HEK-  
733 293T cells grown in DMEM complete medium onto gelatin-coated 100mm dishes. After 8 hours  
734 of incubation at 37°C, the transfection medium was replaced with fresh medium and the  
735 supernatant collected after 24 hours. The medium was replaced again, and a second round of  
736 supernatant was collected after another 24 hours and mixed with the previous batch. The  
737 combined supernatants were centrifuged for 5 min at 300 rcf and filtered through 0.45 $\mu$ m  
738 strainers to remove cell debris. Lentiviral particles were then concentrated by centrifugation for  
739 2 hours at 20,000 rcf (Beckman Coulter, Optima L-100K) in round bottom polypropylene tubes  
740 (Beckman Coulter, Cat#326823). After discarding the supernatants, the lentiviral pellets obtained  
741 from one 150mm dish were thoroughly re-suspended in 80  $\mu$ L of PBS. 10<sup>6</sup> fresh cells were then  
742 collected in 900 $\mu$ L of the respective culture medium and 10 $\mu$ L of lentiviral suspension were  
743 added. Subsequently, the virus-cell mixture was centrifuged at 1,000 rcf for 2 hours at 32°C  
744 (Beckman Coulter, Allegra X- 30R). Infected cells were then cultured as described above and  
745 subsequently FACS-sorted for the establishment of clonal cell lines.

746 **Retrovirus production and infection**

747 Retrovirus constructs were generated as described before (Bussmann et al., 2009). For  
748 production of virus for mouse cells platinum E cells (Cell Biolabs, Cat#RV-101) were transfected.  
749 Platinum A cells (Cell Biolabs, Cat#RV-102) were transfected for human cells. Infection of cells  
750 was performed as previously described (Di Stefano et al., 2014).

751 **Carm1 inhibition experiments with TP064**

752 TP064 (Bio-Techne RD Systems, Bristol, UK) was used to inhibit Carm1 activity as previously  
753 described (Nakayama et al., 2018). For experiments with B cells, these were pre-incubated with  
754 5 $\mu$ M of TP046 24 hours prior to induction with  $\beta$ -est, and treatment with the inhibitor continued  
755 during the time of induction. For the colony forming assay with GMPs, 1-10 $\mu$ M of TP064 was  
756 added to the medium at the time of plating.

757 **Cell purification**

758 Mouse bone marrow cell extraction was performed as previously described (Di Stefano et al.,  
759 2014). Briefly, femurs and tibias of C57BL/6J mice were extracted and crushed on a mortar in  
760 PBS supplemented with 4%FBS and 2 mM EDTA and filtered through 0.45 $\mu$ m strainers (Merck  
761 Millipore, Cat#SLHV033RB). For B cells, bone marrow-derived cells were incubated with  
762 sequentially 0.1 $\mu$ g per 1 million cells of both Fc block and Cd19-Biotin antibody for 10 and 20  
763 minutes respectively, followed by 10  $\mu$ L of magnetic streptavidin microbeads (Miltenyi, Cat#130-  
764 048-101) for an additional 20 minutes. Cd19+ cells were sorted using LS columns (Miltenyi,  
765 Cat#130-042-401). For B cell to macrophage transdifferentiation Cd19+ B cells were infected  
766 with C/EBP $\alpha$ -ER-IRES-hCD4 (WT and mutants) and cultured over MEF feeder cells for 4 days.  
767 Cultured B cells were incubated sequentially with 0.1 $\mu$ g per 1 million cells of both Fc block and  
768 hCD4-Biotin antibody for 10 and 20 minutes respectively, followed by 10  $\mu$ L of magnetic  
769 streptavidin microbeads (Miltenyi, Cat#130-048-101) for an additional 20 minutes. hCD4+ cells  
770 were enriched with LS columns (Miltenyi, Cat#130-042-401).

771 For granulocytes and monocytes, bone marrow-derived cells were incubated sequentially  
772 with 0.1 $\mu$ g per 1 million cells of both Fc block and Mac1-Biotin antibody for 10 and 20 minutes  
773 respectively, followed by 10  $\mu$ L of magnetic streptavidin beads (Miltenyi, Cat#130-048-101) for  
774 an additional 20 minutes. Mac1+ cells were sorted using LS columns (Miltenyi, Cat#130-042-  
775 401) and incubated with Mac1-PE and Ly6g-APC for 20 minutes. Mac1+ Ly6g- (monocytes) and  
776 Mac1+ Ly6g+ cells (granulocytes) were sorted using either FACS Aria or Influx cell sorters.

777 For granulocyte-monocyte progenitors (GMPs), bone marrow-derived cells were lineage-  
778 depleted using a Lineage Cell Depletion Kit (Miltenyi, Cat#130-090-858). Lineage negative cells  
779 were then incubated with Cd34-APC, cKit-APC-Cy7, Sca1-PE-Cy7 and Cd16/32-FITC for 1.5  
780 hours. Sca1- cKit+ Cd34+ Cd16/32+ cells (GMPs) were sorted using either FACS Aria or Influx  
781 cell sorters.

782 For 3T3 NIH fibroblasts cells infected with C/EBP $\alpha$ -ER-IRES-hCD4 (WT and T35A) were  
783 incubated with 0.1 $\mu$ g per 1 million cells of both Fc block and hCD4-Biotin antibody (BD  
784 Pharmingen, Cat#555347) for 10 and 20 minutes respectively, followed by 10  $\mu$ L of magnetic  
785 streptavidin beads (Miltenyi, Cat#130-048-101) for an additional 20 minutes. hCD4+ cells were  
786 purified using LS columns (Miltenyi, Cat#130-042-401).

787 For B lymphoblastic leukemia cells (RCH-ACV) cells stably infected with C/EBP $\alpha$ -ERT2-  
788 IRES-GFP, rtTA-Puro and TetO-Carm1-IRES-TdTomato were induced with 1 $\mu$ g/ml of  
789 doxycycline (Sigma-Aldrich, Cat#D9891). GFP+ and TdTomato+ cells were single cell-sorted  
790 using either FACS Aria or Influx cell sorters.

791 In co-cultures between B cells and feeder cells, non-adherent cells were collected, and joined  
792 with trypsinized adherent cells centrifuged at 300 RCF for 5 minutes. Cells were re-suspended  
793 in 100  $\mu$ L PBS containing 1  $\mu$ g/mL of mouse Fc block for 10 minutes. Conjugated primary  
794 antibodies were added to the blocking solution and cells were further incubated at 4°C in the  
795 dark for 20 minutes. Cells were washed with additional 1mL of PBS and centrifuged at 300 rcf  
796 for 5 minutes. The supernatant was discarded and cells were re-suspended in 500  $\mu$ L of PBS  
797 containing 5  $\mu$ g/mL of DAPI. Samples were processed in a FACS analyzer (LSR II, BD; Fortessa,  
798 BD) with DiVa software and data analyzed using FlowJo software.

799 Antibodies used for cell sorting and flow cytometry are listed in **Table S1**.

## 800 **Phagocytosis assay**

801 After B cell to macrophage transdifferentiation, cells were removed from feeder cells through  
802 differential adherence to tissue culture dishes for 40 minutes. Around 200,000 of the resulting B  
803 cells (or induced macrophages) were plated in each well of a 24-well plate containing 0.01%  
804 poly-L-lysine-treated coverslips (Corning, Cat#354085) in 10% FBS-DMEM supplemented with  
805 IL-3 (Peprotech, Cat#213-13), mCSF-1 (Peprotech, Cat#315-03B) and cultured at 37°C  
806 overnight in the presence of 1:1000 diluted blue fluorescent carboxylated microspheres  
807 (Fluoresbrite, Cat#17458-10). Cells were centrifuged at 1000 RCF for 5 minutes to improve  
808 attachment to the coverslips. The supernatant was removed and the cells were washed once  
809 with PBS.

810 For fixation, 4% PFA was added to the wells for 20 minutes, cells were washed twice with  
811 PBS and cell membranes permeabilized with 0.1% Triton X-100 PBS (0.1% PBST) for 15

812 minutes at room temperature. Cells were blocked using 0.1% PBST with 3% Bovine Serum  
813 Albumin (BSA) for 30-45 minutes. Cells were washed twice in PBS. Actin filaments were  
814 subsequently stained with 1:100 diluted red phalloidin (Alexa Fluor 568, Thermo Fisher Scientific,  
815 Cat#A12380) while DNA was stained with a 1:500 diluted yellow probe (Quant-iT PicoGreen  
816 dsDNA Assay Kit, Thermo Fischer Scientific, Cat#P7589). Cells were incubated with the two  
817 dyes in 0.1% PBST containing 1% BSA at room temperature for 1 hour in the dark and washed  
818 twice with PBS afterwards. Coverslips carrying the attached cells in the well were then recovered  
819 with tweezers and mounted upside-down onto a charged glass slide containing a 14  $\mu$ L drop of  
820 mounting medium (7 $\mu$ L Dako + 7 $\mu$ L 0.1% PBST). Coverslips were sealed with nail polish and  
821 imaged in a Leica TCS SPE inverted confocal microscope.

822 Antibodies used for immunofluorescence and intracellular staining for flow cytometry are  
823 listed in **Table S2**.

#### 824 **Proximity ligation assay (PLA)**

825 Proximity ligation assay was performed using Duolink Orange Kit (Sigma-Aldrich,  
826 Cat#DUO92007). Briefly, after sorting or culturing desired cell populations, 8.000 – 100.000 cells  
827 per well were seeded into 24-well plates containing 0.01% poly-L-lysine (Sigma) treated  
828 coverslips in appropriate medium, centrifuged at 1000 x g for 5 minutes and fixed with 4% PFA  
829 for 15 minutes. Subsequent steps were performed according to the kit's protocol with antibody  
830 concentrations identical to those used for immunofluorescence. Coverslips were mounted using  
831 Fluoroshield mounting medium with DAPI (Abcam, Cat#ab104139) and imaged in a Leica TCS  
832 SPE confocal microscope.

#### 833 **Intracellular staining for flow cytometry**

834 After antibody staining of cell surface markers, cells were fixed in 4% BSA for 10 minutes at room  
835 temperature in a rotating wheel. Fixation was stopped with two washes in PBS. Cells were  
836 permeabilized in 0.1% PBST at room temperature in a rotating wheel for 10 minutes. Cells were  
837 blocked using 0.1% PBST with 3% Bovine Serum Albumin (BSA) for 30-45 minutes. Cells were  
838 washed twice in PBS. Cells were incubated with primary antibodies and secondary antibodies  
839 diluted at the stated concentrations in 0.1% PBST with 1% BSA for 2 and 1 hours, respectively,  
840 with two washes in PBS in between and after. Cells were resuspended in PBS and processed in

841 a FACS analyzer (LSR II, BD; Fortessa, BD) with DiVa software and data analyzed using FlowJo  
842 software.

843 Antibodies used for immunofluorescence and intracellular staining for flow cytometry are  
844 listed in **Table S2**.

845 **Protein extraction, immunoprecipitation and Western blotting**

846 Preparation of whole cell lysates and immunoprecipitation of WT or mutant C/EBP $\alpha$  proteins  
847 were performed as previously described (Kowenz-Leutz et al., 2010). Briefly, cells were lysed  
848 (20 mM HEPES pH 7.8, 150 mM NaCl, 1 mM EDTA pH 8, 10 mM MgCl<sub>2</sub>, 0.1% Triton X-100,  
849 10% Glycerol, protease inhibitor cocktail (Merck), 1mM DTT, 1mM PEFA bloc (Böhringer).  
850 Immunoprecipitation was performed with appropriate antibodies as indicated for 2 h at 4°C.  
851 Immunoprecipitated proteins were collected on Protein A Dynabeads (Invitrogen, Cat#100001D)  
852 or Protein-G Dynabeads (Invitrogen, Cat#10004D), separated by SDS-PAGE (Mini PROTEAN  
853 TGX, 4-15%, Bio-RAD #5671084). For Western blotting, samples were loaded in 10% Mini-  
854 PROTEAN TGX gels (Bio- Rad) and resolved by electrophoresis in running buffer (**Table S3**).  
855 Protein samples were transferred to a methanol pre-activated PVDF membrane (Bio-Rad,  
856 Cat#1620177, Bio-Rad) by running them in transfer buffer (TBS) (**Table S3**) for 1 hour at 300mA  
857 and 4°C. Membranes were rinsed in milliQ water and protein transfer was checked by Ponceau  
858 staining (Sigma). Transferred membranes were washed once with TBS and three times with  
859 TBS- Tween (TBST) (**Table S3**) followed by 5% milk in TBST for 45 min. Membranes were then  
860 incubated with primary antibodies (**Table S4**) in 5% milk TBST, rotating overnight at 4°C, then  
861 washed three times with TBST followed by incubation with the secondary antibodies conjugated  
862 to horseradish peroxidase in 5% milk TBST for 1 hour. After three TBST washes, proteins were  
863 detected using enhanced chemiluminescence reagents (Amersham ECL Prime Western Blotting  
864 detection) in an Amersham Imager 600 analyzer or visualized by ECL (GE Healthcare, UK)..  
865 Quantification of band intensity from scanned blots was performed with Fiji software.

866 **Electrophoretic mobility shift assay**

867 Nuclear extracts were prepared from transfected HEKT cells by a mininuclear extract protocol  
868 (Schreiber et al., 1989). Electrophoretic mobility shift assays (EMSA) was performed as  
869 previously described (Kowenz-Leutz et al., 1994) using double stranded IRDye Oligonucleotides  
870 containing a C/EBP-binding site: IRD800-GACACTGGATTGCGCAATAGGCTC and IRD800-

871 GAGCCTATTGCGCAATCCAGTGTC (Metabion). Briefly, binding reactions with nuclear extracts  
872 (2,5µg) and double stranded IRD800 oligos (20pmol) were incubated for 15 min on ice, orange  
873 loading dye (Li-Cor, Cat# P/N 927-10100) was added and protein-DNA complexes were  
874 separated on a 5% native polyacrylamide gel in 0,5x TBE at 25mA at room temperature. EMSA  
875 results were visualized and quantified (Odyssey scanner, Licor, channel 800nm).

876 ***In vitro* protein methylation assay**

877 Methylation of peptides (PSL, Heidelberg, Germany, **Table S5**) was performed using the  
878 bioluminescence-based MTase-Glo™ Assay (Promega, Cat#V7601) according to the  
879 manufacturer's protocol. Assay conditions: 200 ng of enzyme was incubated with 5µM Peptide,  
880 10 µM S-adenosyl-L-(methyl)-methionine as methyl donor (SAM) and 6x Methyltransferse-Glo  
881 reagent at 23°C for 60 minutes. S-adenosylhomocysteine (SAH) generated during the reaction  
882 was converted to ADP as a proportional reaction product dependent of substrate methylation by  
883 the enzymes. Subsequent incubation with the Methyltransferse-Glo Detection Solution at 23°C  
884 for 30 minutes converts ADP to ATP that is used in a luciferase/luciferin-based reaction and  
885 determined as relative light units (RLU) in a Berthold luminometer (Hsiao et al., 2016).

886 **RNA sequencing**

887 RNA was extracted with a miRNeasy mini kit (217004, Qiagen), quantified with a NanoDrop  
888 spectrophotometer and its quality examined in a fragment Bioanalyzer (Aligent 2100 Bioanalyzer  
889 DNA 7500 assay). cDNA was synthesized with a High-Capacity RNA-to-cDNA kit (4387406,  
890 Applied Biosystems). For RNA-sequencing (RNA-seq), libraries were prepared with a TruSeq  
891 Stranded mRNA Library Preparation Kit (Illumina) followed by single-end sequencing (50 bp) on  
892 a HiSeq2500 instrument (Illumina), obtaining at least 40 million reads per sample.

893 Quality control of FASTQ reads was performed using FastQC version v.0.11.3. Reads  
894 were mapped aligned to the mm10 genome using STAR version 2.5.0a (Dobin et al., 2013).  
895 Gene counts were quantified Gene expression was quantified using STAR (--quantMode  
896 GeneCounts). Normalized counts and differential gene expression analysis was carried out using  
897 DESeq2 version 1.14.1 (Love et al., 2014). For each transdifferentiation experiment, timepoint  
898 0h was set as a reference point and any gene that exhibited a statistically significant change in  
899 expression ( $\log_{2}FC \geq 0.5849625$  and  $p\text{-value} \leq 0.05$ ) at a later timepoint was isolated. For PCA,  
900  $\log_{2}$  DESeq2 normalized counts of differentially expressed genes averaged across replicates

901 were used. The R `prcomp()` command with `scale=T` was used. Pheatmap version 1.0.12 was  
902 used to visualize changes in gene expression for all the isolated differentially expressed genes  
903 with the following clustering options: `clustering_distance_rows="correlation"`,  
904 `clustering_method="ward.D2"`, `scale="row"`.

905 **Scatter plots**

906 Differentially expressed genes (DEGs) were determined for each timepoint as described in  
907 the “Materials and Methods”. The union of identified DEGs in the WT and R35A systems per  
908 timepoint were used to generate scatterplots depicting the log2FC changes of the  
909 aforementioned genes for each transdifferentiation system. A regression line, colored in red, was  
910 fit for each scatterplot using the `geom_smooth(method=lm)` R command. The identity line ( $y=x$   
911 line) is depicted in green. The spearman correlation coefficient (`cor(method="spearman")`  
912 function in R) and the number of DEGs are also depicted per scatterplot.

913 **Gene ontology analysis**

914 Functional analyses by GO were performed with the R package “g:profiler2” version 0.2.0  
915 (Raudvere et al., 2019). Balloonplots depict all pathways associated with a specific keyword that  
916 were found enriched in at least 1 cluster. Metaplots for each cluster depict the average log2FC  
917 values of genes per timepoint and per cluster. Shaded background corresponds to the mean  
918 values  $\pm$  1.644854 standard deviation. Gene expression analysis of signature genes was  
919 performed using the individual values of genes listed in **Table S6** and normalized to timepoints  
920 0h for B cell genes and 120h for macrophage genes.

921 **Chromatin accessibility by ATAC-seq**

922 ATAC-seq was performed as published (Buenrostro et al., 2015). Briefly, cells were harvested  
923 at the mentioned timepoints, feeder-depleted and lysed and 50.000 cells used per condition.  
924 Immediately, transposition was performed using Nextera Tn5 Transposase (15027865, Illumina)  
925 at 37°C for 30 minutes. Chromatin was then purified using Qiagen MinElute PCR Purification Kit  
926 (28004, Qiagen). DNA was then amplified using NEBNext High Fidelity PCR Master Mix  
927 (M0541S, New England Biolabs Inc.) and barcoded primers (see table MMX). qPCR was  
928 performed to determine the optimal number of cycles for each condition to stop amplification prior  
929 to saturation. Quality was analyzed by gel electrophoresis and in a fragment Bioanalyzer (Agilent  
930 2100 Bioanalyzer DNA 7500 assay).

931        Read quality was assessed with FastQC version v.0.11.3. Adaptors were removed using  
932        Cutadapt (version 0.4.2\_dev) TrimGalore! In paired end mode (--paired –nextera)(Martin,  
933        2011).Reads were aligned to the mm10 genome using bowtie2 (v 2.2.4) in paired end mode with  
934        standard parameters. Output SAM files were converted to BAM files using samtools (v 0.1.19)  
935        (Li et al., 2009).BAM files were sorted and indexed using the samtools commands sort and index,  
936        respectively. Low quality reads and reads associated with a not primary or supplementary  
937        alignment SAM flag were filtered out using the samtools command “samtools view -F 2304 -b -q  
938        10”. PCR duplicates were removed with Picard MarkDuplicates (version 2.3.0) with the following  
939        options: “REMOVE\_DUPLICATES=true ASSUME\_SORTED=true VERBOSITY=WARNING”.

940        Filtered BAM files were indexed with samtools index and were used as input in the  
941        bamCoverage command of deeptools (v3.0.1)(Ramírez et al., 2014) in order to generate bigwig  
942        files. bamCoverage was used with the options – binSize 1 –normalizeUsing RPGC –  
943        effectiveGenomeSize 2150570000 –extendReads –outFileFormat bigwig. In order to call peaks,  
944        bam files of each timepoint and experiment were merged using the samtools merge command.  
945        Resulting merged bam files were indexed, and peaks were called using MACS2 with the options  
946        -f BAMPE –nolambda –nomodel -g mm -q 0.05.

#### 947        **Determination of differentially accessible ATAC peaks**

948        In order to pinpoint regions of interest, peaks of all timepoints and all experiments were merged  
949        using the bedtools suite command bedtools merge. Read counts falling within the merged peak  
950        regions were calculated using the Rsubread package and the featurecounts command with the  
951        options isPairedEnd=T, strandSpecific=0, useMetaFeatures=F. For each transdifferentiation  
952        experiment, DESeq2 was used in order to compare all timepoints with timepoint 0h. Any peak  
953        showing a  $\log_{2}FC \geq 1$  & Adjusted p-value  $\leq 0.05$  & average counts across timepoints  $\geq 5$  was  
954        termed as a differentially accessible region and was kept for further analyses. The total number  
955        of peaks isolated was 91830. Variance stabilized counts were calculated for the isolated regions  
956        using the DESeq2 command varianceStabilizingTransformation and the options “blind=T”,  
957        fitType=“parametric”. Variance stabilized counts were averaged across timepoint replicates by  
958        raising them at the power of 2, extracting their average and log2 transforming the resulting mean.  
959        PCA was applied to this dataset using the R prcomp command, with “scale=T”.

960 To group peaks, PCA was initially applied and PC1 and PC2 values for the 91,830 regions  
961 were used in order to arbitrary cluster peaks into 3 groups depending on the sign of their PC1  
962 and PC2 values. Values for each of the 3 groups were visualized using the pheatmap package.  
963 Visual examination of the 3 main groups showed different trends: Peaks whose accessibility is  
964 higher at 120h (43429 peaks), is lower at 120h (36380 peaks) and is higher at 18h (12021 peaks).

965 **Motif analysis**

966 Peaks from the 3 different groups were centered and extended 50bp upstream and downstream.  
967 Nucleotide sequences for each centered peak were extracted using bedtools getfasta.  
968 Sequences were submitted into MEME-ChIP with the following parameters: -dna -seed 49 -  
969 meme-nmotifs 20 -meme-minw 5 -meme-minsites 2 -meme-minw 4 -meme-maxw 12. TOMTOM  
970 was run using the output meme.txt file in order to identify matches of known transcription factor  
971 motifs to the *de novo* discovered motifs. For each TOMTOM output a series of additional filtering  
972 steps were undertaken:

- 973 1. *De novo* motif sequences need to have  $\leq 75\%$  rate for each nucleotide (filtering out  
974 repetitive motifs).
- 975 2. TOMTOM q-values have to be  $\leq 0.01$ .
- 976 3. The matched transcription factor has to be expressed at least at one timepoint.

977 **Promoter accessibility analysis**

978 Genomic coordinates of mm10 genes were downloaded from the UCSC table browser (RefSeq  
979 genes). A single promoter region was assigned to each gene. The region consisted of 1kb  
980 upstream and downstream of the transcription start site of the largest transcript of each gene.  
981 Counts for each timepoint and each transdifferentiation experiment were assigned to each  
982 promoter as described above. DESeq2 was used in order to identify differentially accessible  
983 promoters as described above with the following differences regarding the cutoffs used:  
984 FoldChange $\geq 1.5$  & p-value  $\leq 0.05$ . Variance stabilized counts were extracted for each  
985 differentially accessible promoter, a mean value per replicate was extracted and the values were  
986 plotted using pheatmap. Promoters were then grouped into 8 clusters. Balloonplots depict all  
987 pathways associated with a specific keyword that were found enriched in at least 1 cluster.

988 For each promoter cluster and each promoter, log2FC changes were extracted by comparing  
989 expression levels (DESeq2 normalized counts) of every timepoint with the corresponding  
990 timepoint 0h of the experiment.

## 991 **Virtual ChIP**

992 C/EBP $\alpha$  and PU.1 binding profiles from ChIP-seq experiments in mouse B cell to macrophage  
993 transdifferentiation system were retrieved from earlier work (Van Oevelen et al., 2015). C/EBP $\alpha$   
994 and PU.1 peaks from timepoints 0h, 3h, 12h and 24h were pooled and merged using the bedtools  
995 merge command. Each peak was assigned a unique identifier corresponding to the timepoints  
996 and experiments the peak was “present”. 6 different groups of peaks were extracted from the  
997 pooled file:

998 1, 2 and 3.\_Peaks bound by PU.1 at 0h but not at 24h. Group was split further into two sub-  
999 groups depending on whether C/EBP $\alpha$  was found to bind at any timepoint.

1000 4, 5 and 6.\_Peaks bound by C/EBP $\alpha$  at 24h but not at 0h. Group was split further into two  
1001 sub-groups depending on whether PU.1 was found to bind at any timepoint.

1002 Three different kinds of plots were used to summarize the accessibility dynamics of the six  
1003 group of peaks in our transdifferentiation system. For each peak the average ATAC-seq bigwig  
1004 score was calculated using deeptools multiBigwigSummary. Any peak overlapping with mm10  
1005 encode blacklisted regions was excluded. Values were averaged across timepoint replicates and  
1006 visualized in R using the pheatmap package. The same values used for the heatmap peak values  
1007 were used. Z-transformed values were calculated for every peak.

## 1008 **Single molecule tracking (SMT)**

1009 30,000 NIH 3T3 cells inducible for CEBPAwt-HALO or CEBPAr35a-HALO were seeded in a  
1010 LabTek-II chambered 8 well plates (Lab-Tek 155049), and induced for 6h or 24h with 1ug/ml  
1011 doxycycline, with or without prior infection with TETO-FUW-PU.1 lentivirus infection. Right before  
1012 imaging, cells were treated with 5nM of Janelia Fluor 549 (JF549) HaloTag ligand (a kind gift  
1013 from Luke Lavis, HHMI) for 15 minutes. Cells were subsequently washed three times in PBS at  
1014 37C, and Phenol Red-free High Glucose medium was added to each well. All imaging was  
1015 carried out under HILO conditions (Tokunaga et al., 2008). For imaging experiments, one frame  
1016 was acquired with 100ms of exposure time (10 Hz) to measure the intensity of fluorescence of

1017 the nuclei, and in SMT) experiments, 5000 frames were acquired with an exposure of 10ms (100  
1018 Hz).

1019 Imaging experiments were carried out in Phenol red-free High Glucose Medium  
1020 (ThermoFisher, Cat#21063029) pyruvate, GlutaMAX, in an imaging chamber heated at 37°C  
1021 (more details in the Single Molecule Live Cell Imaging section). All live-cell imaging experiments  
1022 of SMT were carried out in a Nanoimager S from Oxford Nanoimaging Limited (ONI), in a  
1023 temperature and humidity-controlled chamber, a scientific Complementary metal-oxide-  
1024 semiconductor (sCMOS) camera with a 2.3 electrons rms read noise at standard scan, a 100X,  
1025 1.49 NA oil immersion objective and a 561 nm green laser. Images were acquired with the  
1026 Nanoimager software. Quantification and Statistical Analysis of SMT was performed as  
1027 previously described (Lerner et al., 2020). All scripts are publicly available.

## 1028 **Two Parameter SMT Tracking Analysis**

1029 In brief, TIF stacks SMT movies were analyzed using MATLAB-based SLIMfast script (Teves et  
1030 al., 2016) a modified version of MTT (Sergé et al., 2008), with a Maximal expected Diffusion  
1031 Coefficient (DMax) of 3  $\mu\text{m}^2/\text{s-1}$ . The SLIMfast output .txt files were reorganized by the  
1032 homemade csv\_converter.m MATLAB script (available in (Lerner et al., 2020) in .csv format for  
1033 further analysis. The single molecule tracking .csv files (see previous section) were first classified  
1034 by the homemade SMT\_Motion\_Classifier.m MATLAB script. Single molecule trajectories (or  
1035 tracks) with a track duration shorter than 5 frames were discarded from the analysis. Motion  
1036 tracks are classified by the script in different groups: tracks with  $\alpha \leq 0.7$  were considered as  
1037 Confined; motion tracks with  $0.7 < \alpha < 1$  as Brownian; and motion tracks with  $\alpha \geq 1$  as Directed.  
1038 In addition, the motion tracks showing a behavior similar to a levy-flight (presenting mixed  
1039 Confined and Directed/Brownian behavior) were detected by the presence of a jump superior to  
1040 the average jump among the track + a jump threshold of 1.5, and classified as “Butterfly.” Butterfly  
1041 motion tracks were segmented into their corresponding Confined and Directed/Brownian sub-  
1042 trajectories for posterior analysis. As an additional filtering step of confined motions (including  
1043 confined segments of Butterfly tracks), we defined a jump threshold of 100nm, to filter out motion  
1044 tracks with an average frame-to-frame jump size larger than 100nm.

## 1045 **Data mining of published datasets**

1046 DNA-binding peaks of C/EBP $\alpha$  and PU.1 during BMT were extracted from (Van Oevelen et al.  
1047 2015) and analysed as stated above. Single-cell expression trajectories and correlations in B cell  
1048 transdifferentiation and reprogramming were processed from (Francesconi et al., 2019). Gene  
1049 expression data from hematopoietic cells (CMP, GMP, Monocyte and Granulocyte (neutrophil))  
1050 were from (Ohlsson et al., 2016).

1051 **Statistical analyses**

1052 Statistical analyses were performed using Prism 9 software. To calculate significance, samples  
1053 from at least 3 biologically independent experiments were analyzed. Two biological replicates  
1054 were used for RNA- and ATAC- sequencing experiments and statistics applied to the expression  
1055 of a collection of genes. For samples with  $n \geq 3$ , values shown in the figures represent mean  $\pm$   
1056 standard deviation. Box plots represent median with quartiles and whiskers and individual values  
1057 are shown. One-way, two-way ANOVA (with the corresponding multiple comparison analyses)  
1058 and Student's t-tests were applied accordingly. P-values appear indicated in each figure only  
1059 when  $\leq 0.05$ . In time-course experiments, p-values of differences between conditions by two-  
1060 way ANOVA are shown. In box plots, p-values of each individual timepoint as well as p-values  
1061 of differences between conditions by two-way ANOVA are shown.

1062

1063 **Table S1. List of antibodies used for cell sorting and Flow cytometry experiments**

| FACS/Cell sorting   |                |           |         |          |
|---------------------|----------------|-----------|---------|----------|
| Antibody            | Company        | Catalogue | Species | Dilution |
| Cd16/Cd32 (FcBlock) | BD Pharmingen  | 553142    | Rat     | 1:400    |
| Cd19-Biotin         | BD Biosciences | 553784    | Rat     | 1:400    |
| Mac1-Biotin         | BD Pharmingen  | 557395    | Rat     | 1:400    |
| hCD4-Biotin         | eBioscience    | 13-0049   | Mouse   | 1:33     |
| Cd19-APC            | BD Pharmingen  | 550992    | Rat     | 1:400    |
| Mac1-PE-Cy7         | BD Pharmingen  | 552850    | Rat     | 1:400    |
| Ly6g-PE             | Pharmingen     | 553128    | Rat     | 1:400    |

|                          |               |            |       |       |
|--------------------------|---------------|------------|-------|-------|
| Mac1-APC                 | eBioscience   | 17-0112-83 | Rat   | 1:400 |
| hCD4-PE                  | BD Pharmingen | 555347     | Mouse | 1:20  |
| hCD16/CD32<br>(hFcBlock) | Invitrogen    | 16-9161-73 | -     | 1:20  |
| hCD19-APC-Cy7            | BD Pharmingen | 557791     | Mouse | 1:33  |
| hMac1-APC                | BD Pharmingen | 561015     | Mouse | 1:33  |
| Cd16/Cd32-FITC           | BD Pharmingen | 553144     | Rat   | 1:400 |
| cKit-APC-Cy7             | Invitrogen    | 47-1172-82 | Rat   | 1:400 |
| Cd34-APC                 | BD Pharmingen | 560230     | Rat   | 1:50  |
| Sca1-PE-Cy7              | BD Pharmingen | 558162     | Rat   | 1:400 |
| Sca1-PerCP-Cy5.5         | eBioscience   | 35-5981-82 | Rat   | 1:400 |
| Cd41-PE-Cy7              | eBioscience   | 25-0411-82 | Rat   | 1:400 |

1064

1065 **Table S2. List of antibodies and fluorochromes used for immunofluorescence and**  
1066 **intracellular staining for flow cytometry**

| Intracellular staining for flow cytometry |                |           |         |          |
|---|----------------|-----------|---------|----------|
| Antibody                                  | Company        | Catalogue | Species | Dilution |
| C/EBP $\alpha$                            | Cell Signaling | 8178      | Rabbit  | 1:100    |
| Carm1                                     | Cell Signaling | 12495     | Mouse   | 1:100    |
| PU.1                                      | Abcam          | Ab88082   | Mouse   | 1:100    |
| BAFF155                                   | Cell Signaling | D7F8S     | Rabbit  | 1:200    |
| BAFF155-<br>AsDM                          | Cell Signaling | 94962     | Rabbit  | 1:200    |
| AF488 Anti-<br>rabbit                     | ThermoFisher   | A-11070   | Goat    | 1:500    |

|                  |              |         |      |       |
|------------------|--------------|---------|------|-------|
| AF555 Anti-mouse | ThermoFisher | A-21422 | Goat | 1:500 |
|------------------|--------------|---------|------|-------|

1067

1068 **Table S3. Chemical reagents used to prepare buffers for western blot.**

| Running buffer | Transfer buffer         | TBST              |
|----------------|-------------------------|-------------------|
| 25mM Tris-base | 25mM Tris-HCl<br>pH=3.8 | 10mM Tris HCl=7.5 |
| 200mM glycine  | 200mM glycine           | 100mM NaCl        |
| 0.1% SDS       | 20% methanol            | 0.1% Tween 20     |

1069 **Table S4. List of antibodies used for western blot experiments**

| Antibody       | Company        | Catalogue | Species | Dilution |
|----------------|----------------|-----------|---------|----------|
| C/EBP $\alpha$ | Cell Signaling | 8178      | Rabbit  | 1:1000   |
| aDMA           | Cell Signaling | 13522S    | Rabbit  | 1:1000   |
| aDMA           | Upstate        | #07-414   | Rabbit  | 1:1000   |
| HA             | Covance        | #MMS-101R | Mouse   | 1:1000   |
| Flag           | Sigma          | F3165     | Mouse   | 1:1000   |
| Flag           | Abnova         | PAB 29056 | Chicken | 1:1000   |
| BAFF155        | Cell Signaling | D7F8S     | Rabbit  | 1:1000   |
| BAFF155-AsDM   | Cell Signaling | 94962     | Rabbit  | 1:1000   |
| PU.1           | Abcam          | Ab88082   | Mouse   | 1:1000   |
| Vinculin       | Merck          | V9131     | Mouse   | 1:200    |

|       |       |         |       |        |
|-------|-------|---------|-------|--------|
| Gapdh | Abcam | Ab8245  | Mouse | 1:5000 |
| H3    | Abcam | Ab10799 | Mouse | 1:1000 |

1070

1071 **Table S5. List of peptides used for in vitro methylation experiments**

| Peptides  |
|---|
| YEAEP <b>R</b> PPMSS, aa 7-17                                 |
| AFGFP <b>R</b> GAGPA, aa 30-40                                |
| LFQHS <b>R</b> QQEKA, aa 81-91                                |
| GYLDG <b>R</b> LEPLY, aa 137-147                              |
| EPLYE <b>R</b> VGAPA, aa 144-154                              |
| GAPAL <b>R</b> PLVIK, aa 151-161                              |
| IKQEP <b>R</b> EEDEA, aa 160-170                              |
| AHPDL <b>R</b> ASGGS, aa 259-269                              |
| SNEY <b>R</b> VRRE <b>R</b> NNIA, aa 282-295                  |
| NIAV <b>R</b> KSRDKAK, aa 293-304                             |
| DKAKQ <b>R</b> NVETQ, aa 301-311                              |
| SDND <b>R</b> L <b>R</b> K <b>R</b> VEQL, aa 319-331          |
| VEQLS <b>R</b> ELDTL, aa 328-338                              |
| ELDTL <b>R</b> GIF <b>R</b> QLPES, aa 334-348                 |
| MSSHLSPPHAPSSAAFGFP <b>R</b> GAGP<br>AQPPAPPAAPEPLGG aa 15-54 |

|   |
|---|
| MSSHLSPPHAPSSAAF <sup>GF</sup> <sup>P</sup> <sup>R(me2)</sup> |
| GAGPAQPPAPPAAPEPLGG aa 15-54                                  |
| MSSHLSPPHAPSSAAF <sup>GF</sup> <sup>P</sup> <sup>R/AGA</sup>  |
| GPAQPPAPPAAPEPLGG aa 15-54                                    |
| PRMT4 peptide substrate                                       |
| Histone H3 aa 1-21  |
| Histone H4 aa 1-21  |

1072

1073 **Table S6. List of genes used to analyze kinetics of specific signatures**

**B cell genes – Figure S1H**

*Pax5, Ebf1, Foxo1, Iκzf1, Rag1, Rag2, Bcl11a, Spib, Iκzf3, Cd2, Cd19, Igll1, Vpreb1, Vpreb2, Vpreb3, Pou2a1, Blk, Cd79a, Cd79b, Lef1*

**Macrophage genes – Figure S1H**

*C1qc, Fcer1g, Sell, Ccr1, Mitf, Tlr2, Csf1r, Trem2, Fam20c, Adam8, Batf2, Fes, Itgam, Ccl3, Cd300lf, Tnsf9, Tyrobp, Cd14, Ifitm6, Csf3r*

1074

1075 **Newly Created Materials**

1076 The new constructs and cell lines listed can be requested from the corresponding authors. The  
1077 sequencing data will be deposited at GEO and made freely available

1078 **Competing interests**

1079 The authors declare no competing interests

1080 **REFERENCES**

- 1081 Arinobu Y, Mizuno S, Chong Y, Shigematsu H, Iino T, Iwasaki H, Graf T, Mayfield R, Chan S,  
1082 Kastner P, Akashi K. 2007. Reciprocal Activation of GATA-1 and PU.1 Marks Initial  
1083 Specification of Hematopoietic Stem Cells into Myeloerythroid and Myelolymphoid Lineages.  
1084 *Cell Stem Cell* **1**:416–427. doi:10.1016/j.stem.2007.07.004
- 1085 Bedford MT, Clarke SG. 2009. Protein Arginine Methylation in Mammals: Who, What, and Why.  
1086 *Mol Cell* **33**:1–13. doi:10.1016/j.molcel.2008.12.013
- 1087 Bedford MT, Richard S. 2005. Arginine methylation: An emerging regulator of protein function.  
1088 *Mol Cell* **18**:263–272. doi:10.1016/j.molcel.2005.04.003
- 1089 Buenrostro JD, Wu B, Chang HY, Greenleaf WJ. 2015. ATAC-seq: A method for assaying  
1090 chromatin accessibility genome-wide. *Curr Protoc Mol Biol* **2015**:21.29.1-21.29.9.  
1091 doi:10.1002/0471142727.mb2129s109
- 1092 Bussmann LH, Schubert A, Vu Manh TP, De Andres L, Desbordes SC, Parra M, Zimmermann  
1093 T, Rapino F, Rodriguez-Ubreva J, Ballestar E, Graf T. 2009. A Robust and Highly Efficient  
1094 Immune Cell Reprogramming System. *Cell Stem Cell* **5**:554–566.  
1095 doi:10.1016/j.stem.2009.10.004
- 1096 Cai DH, Wang D, Keefer J, Yeaman C, Hensley K, Friedman AD. 2008. C/EBP $\alpha$ :AP-1 leucine  
1097 zipper heterodimers bind novel DNA elements, activate the PU.1 promoter and direct  
1098 monocyte lineage commitment more potently than C/EBP $\alpha$  homodimers or AP-1. *Oncogene*  
1099 **27**:2772–2779. doi:10.1038/SJ.ONC.1210940
- 1100 Chang NC, Sincennes MC, Chevalier FP, Brun CE, Lacaria M, Segalés J, Muñoz-Cánores P,  
1101 Ming H, Rudnicki MA. 2018. The Dystrophin Glycoprotein Complex Regulates the  
1102 Epigenetic Activation of Muscle Stem Cell Commitment. *Cell Stem Cell* **22**:755–768.e6.  
1103 doi:10.1016/j.stem.2018.03.022
- 1104 Chen J, Zhang Z, Li L, Chen BC, Revyakin A, Hajj B, Legant W, Dahan M, Lionnet T, Betzig E,  
1105 Tjian R, Liu Z. 2014. Single-molecule dynamics of enhanceosome assembly in embryonic  
1106 stem cells. *Cell* **156**:1274–1285. doi:10.1016/j.cell.2014.01.062
- 1107 Choi J, Baldwin TM, Wong M, Bolden JE, Fairfax KA, Lucas EC, Cole R, Biben C, Morgan C,  
1108 Ramsay KA, Ng AP, Kauppi M, Corcoran LM, Shi W, Wilson N, Wilson MJ, Alexander WS,  
1109 Hilton DJ, De Graaf CA. 2019. Haemopedia RNA-seq: A database of gene expression during  
1110 haematopoiesis in mice and humans. *Nucleic Acids Res* **47**:D780–D785.  
1111 doi:10.1093/nar/gky1020
- 1112 Deribe YL, Pawson T, Dikic I. 2010. Post-translational modifications in signal integration. *Nat  
1113 Struct Mol Biol* **17**:666–672. doi:10.1038/nsmb.1842
- 1114 Di Stefano B, Sardina JL, Van Oevelen C, Collombet S, Kallin EM, Vicent GP, Lu J, Thieffry D,  
1115 Beato M, Graf T. 2014. C/EBP $\alpha$  poised B cells for rapid reprogramming into induced  
1116 pluripotent stem cells. *Nature* **506**:235–239. doi:10.1038/nature12885
- 1117 Dobin A, Davis CA, Schlesinger F, Drenkow J, Zaleski C, Jha S, Batut P, Chaisson M, Gingeras  
1118 TR. 2013. STAR: Ultrafast universal RNA-seq aligner. *Bioinformatics* **29**:15–21.  
1119 doi:10.1093/bioinformatics/bts635
- 1120 Ebisuya M, Briscoe J. 2018. What does time mean in development? *Development* **145**.  
1121 doi:10.1242/dev.164368

- 1122 Eyquem S, Chemin K, Fasseu M, Chopin M, Sigaux F, Cumano A, Bories JC. 2004. The  
1123 development of early and mature B cells is impaired in mice deficient for the Ets-1  
1124 transcription factor. *Eur J Immunol* **34**:3187–3196. doi:10.1002/EJI.200425352
- 1125 Feng R, Desbordes SC, Xie H, Tillo ES, Pixley F, Stanley ER, Graf T. 2008. PU.1 and C/EBP $\alpha$ / $\beta$   
1126 convert fibroblasts into macrophage-like cells. *Proceedings of the National Academy of  
1127 Sciences* **105**:6057–6062. doi:10.1073/pnas.0711961105
- 1128 Fernandez Garcia M, Moore CD, Schulz KN, Alberto O, Donague G, Harrison MM, Zhu H, Zaret  
1129 KS. 2019. Structural Features of Transcription Factors Associating with Nucleosome  
1130 Binding. *Mol Cell* **75**:921-932.e6. doi:10.1016/j.molcel.2019.06.009
- 1131 Francesconi M, di Stefano B, Berenguer C, Andrés-Aguayo L de, Plana-Carmona M, Mendez-  
1132 Lago M, Guillaumet-Adkins A, Rodriguez-Esteban G, Gut M, Gut IG, Heyn H, Lehner B, Graf  
1133 T. 2019. Single cell RNA-seq identifies the origins of heterogeneity in efficient cell  
1134 transdifferentiation and reprogramming. *eLife* **8**:1–22. doi:10.7554/eLife.41627
- 1135 Graf T, Enver T. 2009. Forcing cells to change lineages. *Nature* **462**:587–594.  
1136 doi:10.1038/nature08533
- 1137 Greenblatt SM, Man N, Hamard PJ, Asai T, Karl D, Martinez C, Bilbao D, Stathais V, McGrew-  
1138 Jermacowicz A, Duffort S, Tadi M, Blumenthal E, Newman S, Vu L, Xu Y, Liu F, Schurer  
1139 SC, McCabe MT, Kruger RG, Xu M, Yang FC, Tenen D, Watts J, Vega F, Nimer SD. 2018.  
1140 CARM1 Is Essential for Myeloid Leukemogenesis but Dispensable for Normal  
1141 Hematopoiesis. *Cancer Cell* **33**:1111-1127.e5. doi:10.1016/j.ccr.2018.05.007
- 1142 Guo Z, Zheng L, Xu H, Dai H, Zhou M, Pascua MR, Chen QM, Shen B. 2010. Methylation of  
1143 FEN1 suppresses nearby phosphorylation and facilitates PCNA binding. *Nat Chem Biol*  
1144 **6**:766–773. doi:10.1038/NCHEMBO.422
- 1145 Heath V, Suh HC, Holman M, Renn K, Gooya JM, Parkin S, Klarmann KD, Ortiz M, Johnson P,  
1146 Keller J. 2004. C/EBP $\alpha$  deficiency results in hyperproliferation of hematopoietic progenitor  
1147 cells and disrupts macrophage development in vitro and in vivo. *Blood* **104**:1639–1647.  
1148 doi:10.1182/blood-2003-11-3963
- 1149 Heinz S, Benner C, Spann N, Bertolino E, Lin YC, Laslo P, Cheng JX, Murre C, Singh H, Glass  
1150 CK. 2010. Simple Combinations of Lineage-Determining Transcription Factors Prime cis-  
1151 Regulatory Elements Required for Macrophage and B Cell Identities. *Mol Cell* **38**:576–589.  
1152 doi:10.1016/j.molcel.2010.05.004
- 1153 Hertweck A, Mucha MV De, Barber PR, Dagil R, Porter H, Ramos A, Lord GM, Jenner RG. 2022.  
1154 The TH1 cell lineage-determining transcription factor T-bet suppresses TH2 gene  
1155 expression by redistributing GATA3 away from TH2 genes. *Nucleic Acids Res* **1**.  
1156 doi:<https://doi.org/10.1093/nar/gkac258>
- 1157 Hosokawa H, Ungerbäck J, Wang X, Matsumoto M, Nakayama KI, Cohen SM, Tanaka T,  
1158 Rothenberg E V. 2018. Transcription Factor PU.1 Represses and Activates Gene  
1159 Expression in Early T Cells by Redirecting Partner Transcription Factor Binding. *Immunity*  
1160 **48**:1119-1134.e7. doi:10.1016/j.jimmuni.2018.04.024
- 1161 Hsiao K, Zegzouti H, Goueli SA. 2016. Methyltransferase-Glo: A universal, bioluminescent and  
1162 homogenous assay for monitoring all classes of methyltransferases. *Epigenomics* **8**:321–  
1163 339. doi:10.2217/EPI.15.113

- 1164 Hu C-J, Rao S, Ramirez-Bergeron DL, Garrett-Sinha LA, Gerondakis S, Clark MR, Simo MC.  
1165 2001. PU.1/Spi-B Regulation of c-rel Is Essential for Mature B Cell Survival. *Immunity*  
1166 **15**:545–555.
- 1167 Jack I, Seshadri R, Garson M, Michael P, Callen D, Zola H, Morley A. 1986. RCH-ACV: A  
1168 lymphoblastic leukemia cell line with chromosome translocation 1;19 and trisomy 8. *Cancer*  
1169 *Genet Cytogenet* **19**:261–269. doi:10.1016/0165-4608(86)90055-5
- 1170 Kawabe YI, Wang YX, McKinnell IW, Bedford MT, Rudnicki MA. 2012. Carm1 regulates Pax7  
1171 transcriptional activity through MLL1/2 recruitment during asymmetric satellite stem cell  
1172 divisions. *Cell Stem Cell* **11**:333–345. doi:10.1016/j.stem.2012.07.001
- 1173 Kim D, Lee J, Cheng D, Li J, Carter C, Richie E, Bedford MT. 2010. Enzymatic activity is required  
1174 for the in Vivo functions of CARM1. *Journal of Biological Chemistry* **285**:1147–1152.  
1175 doi:10.1074/jbc.M109.035865
- 1176 Klemm SL, Shipony Z, Greenleaf WJ. 2019. Chromatin accessibility and the regulatory  
1177 epigenome. *Nature Reviews* **20**:207–220. doi:10.1038/s41576-018-0089-8
- 1178 Konstantinides N, Holguera I, Rossi AM, Escobar A, Dudragne L, Chen Y-C, Tran TN, Martínez  
1179 Jaimes AM, Öznel MN, Simon F, Shao Z, Tsankova NM, Fullard JF, Walldorf U, Roussos P,  
1180 Desplan C. 2022. A complete temporal transcription factor series in the fly visual system.  
1181 *Nature* **604**:316–322. doi:10.1038/s41586-022-04564-w
- 1182 Kowenz-Leutz E, Pless O, Dittmar G, Knoblich M, Leutz A. 2010. Crosstalk between C/EBPB  
1183 phosphorylation, arginine methylation, and SWI/SNF/Mediator implies an indexing  
1184 transcription factor code. *EMBO Journal* **29**:1105–1115. doi:10.1038/emboj.2010.3
- 1185 Kowenz-Leutz E, Twamley G, Ansieau S, Leutz A. 1994. Novel mechanism of C/EBP $\beta$  (NF-M)  
1186 transcriptional control: Activation through derepression. *Genes Dev* **8**:2781–2791.  
1187 doi:10.1101/gad.8.22.2781
- 1188 Kueh HY, Champhekar A, Nutt SL, Elowitz MB, Rothenberg E v. 2013. Positive Feedback  
1189 Between PU.1 and the Cell Cycle Controls Myeloid Differentiation. *Science (1979)* **341**:670–  
1190 673. doi:10.1126/science.1240831
- 1191 Laiosa C V., Stadtfeld M, Xie H, de Andres-Aguayo L, Graf T. 2006. Reprogramming of  
1192 Committed T Cell Progenitors to Macrophages and Dendritic Cells by C/EBP $\alpha$  and PU.1  
1193 Transcription Factors. *Immunity* **25**:731–744. doi:10.1016/j.jimmuni.2006.09.011
- 1194 Leddin M, Perrod C, Hoogenkamp M, Ghani S, Assi S, Heinz S, Wilson NK, Follows G, Schönheit  
1195 J, Vockentanz L, Mosammam AM, Chen W, Tenen DG, Westhead DR, Göttgens B, Bonifer  
1196 C, Rosenbauer F. 2011. Two distinct auto-regulatory loops operate at the PU.1 locus in B  
1197 cells and myeloid cells. *Blood* **117**:2827–2838. doi:10.1182/blood-2010-08-302976
- 1198 Lerner J, Gomez-Garcia PA, McCarthy RL, Liu Z, Lakadamyali M, Zaret KS. 2020. Two-  
1199 Parameter Mobility Assessments Discriminate Diverse Regulatory Factor Behaviors in  
1200 Chromatin. *Mol Cell* **79**:677–688. doi:10.1016/j.molcel.2020.05.036
- 1201 Li H, Handsaker B, Wysoker A, Fennell T, Ruan J, Homer N, Marth G, Abecasis G, Durbin R.  
1202 2009. The Sequence Alignment/Map format and SAMtools. *Bioinformatics* **25**:2078–2079.  
1203 doi:10.1093/bioinformatics/btp352

- 1204 1205 1206 Li J, Zhao Z, Carter C, Ehrlich LIR, Bedford MT, Richie ER. 2013. Coactivator-Associated  
Arginine Methyltransferase 1 Regulates Fetal Hematopoiesis and Thymocyte Development.  
*The Journal of Immunology* **190**:597–604. doi:10.4049/jimmunol.1102513
- 1207 1208 Liu Z, Tjian R. 2018. Visualizing transcription factor dynamics. *Journal of Cell Biology* **217**:1181–  
1191. doi:10.1083/jcb.201710038
- 1209 1210 Love MI, Huber W, Anders S. 2014. Moderated estimation of fold change and dispersion for  
RNA-seq data with DESeq2. *Genome Biol* **15**:1–21. doi:10.1186/s13059-014-0550-8
- 1211 1212 1213 1214 Ma O, Hong S, Guo H, Ghiaur G, Friedman AD. 2014. Granulopoiesis Requires Increased  
C/EBP $\alpha$  Compared to Monopoiesis, Correlated with Elevated Cebpa in Immature G-CSF  
Receptor versus M-CSF Receptor Expressing Cells. *PLoS One* **9**:e95784.  
doi:10.1371/journal.pone.0095784
- 1215 1216 Martin M. 2011. Cutadapt removes adapter sequences from high-throughput sequencing reads.  
*EMBnet J* **17**.1
- 1217 1218 Moris N, Pina C, Arias AM. 2016. Transition states and cell fate decisions in epigenetic  
landscapes. *Nat Rev Genet* **17**:693–703. doi:10.1038/nrg.2016.98
- 1219 1220 1221 1222 1223 Nakayama K, Szewczyk MM, dela Sena C, Wu H, Dong A, Zeng H, Li F, Ferreira De Freitas R,  
Eram MS, Schapira M, Baba Y, Kunitomo M, Cary DR, Tawada M, Ohashi A, Imaeda Y,  
Singh Saikatendu K, Grimshaw CE, Vedadi M, Arrowsmith CH, Barsyte-Lovejoy D, Kiba A,  
Tomita D, Brown PJ. 2018. TP-064, a potent and selective small molecule inhibitor of  
PRMT4 for multiple myeloma. *Oncotarget* **9**:18480–18493.
- 1224 1225 1226 Nerlov C. 2007. The C/EBP family of transcription factors: a paradigm for interaction between  
gene expression and proliferation control. *Trends Cell Biol* **17**:318–324.  
doi:10.1016/j.tcb.2007.07.004
- 1227 1228 1229 1230 Notta F, Zandi S, Takayama N, Dobson S, Gan OI, Wilson G, Kaufmann KB, McLeod J, Laurenti  
E, Dunant CF, McPherson JD, Stein LD, Dror Y, Dick JE. 2016. Distinct routes of lineage  
development reshape the human blood hierarchy across ontogeny. *Science (1979)* **351**.  
doi:10.1126/science.aab2116
- 1231 1232 Ohlsson E, Schuster MB, Hasemann M, Porse BT. 2016. The multifaceted functions of C/EBP $\alpha$   
in normal and malignant haematopoiesis. *Leukemia*. doi:10.1038/leu.2015.324
- 1233 1234 1235 Okawa S, Saltó C, Ravichandran S, Yang S, Toledo EM, Arenas E, Del Sol A. 2018.  
Transcriptional synergy as an emergent property defining cell subpopulation identity enables  
population shift. *Nat Commun* **9**:1–10. doi:10.1038/s41467-018-05016-8
- 1236 1237 Orkin SH, Zon LI. 2008. Hematopoiesis: An Evolving Paradigm for Stem Cell Biology. *Cell*  
**132**:631–644. doi:10.1016/j.cell.2008.01.025
- 1238 1239 1240 1241 Ramberger E, Sapozhnikova V, Kowenz-Leutz E, Zimmermann K, Nicot N, Nazarov P v., Perez-  
Hernandez D, Reimer U, Mertins P, Dittmar G, Leutz A. 2021. PRISMA and BiOID disclose  
a motifs-based interactome of the intrinsically disordered transcription factor C/EBP $\alpha$ .  
*iScience* **24**:102686. doi:10.1016/j.isci.2021.102686
- 1242 1243 Ramírez F, Dündar F, Diehl S, Grüning BA, Manke T. 2014. DeepTools: A flexible platform for  
exploring deep-sequencing data. *Nucleic Acids Res* **42**:187–191. doi:10.1093/nar/gku365

- 1244 Rapino F, Robles EF, Richter-Larrea JA, Kallin EM, Martinez-Climent JA, Graf T. 2013. C/EBP $\alpha$   
1245 Induces Highly Efficient Macrophage Transdifferentiation of B Lymphoma and Leukemia  
1246 Cell Lines and Impairs Their Tumorigenicity. *Cell Rep* **3**:1153–1163.  
1247 doi:10.1016/j.celrep.2013.03.003
- 1248 Raschke WC, Baird S, Ralph P, Nakoinz I. 1978. Functional macrophage cell lines transformed  
1249 by abelson leukemia virus. *Cell* **15**:261–267. doi:10.1016/0092-8674(78)90101-0
- 1250 Raudvere U, Kolberg L, Kuzmin I, Arak T, Adler P, Peterson H, Vilo J. 2019. G:Profiler: A web  
1251 server for functional enrichment analysis and conversions of gene lists (2019 update).  
1252 *Nucleic Acids Res* **47**:W191–W198. doi:10.1093/nar/gkz369
- 1253 Rayon T, Stamatakis D, Perez-Carrasco R, Garcia-Perez L, Barrington C, Melchionda M, Exelby  
1254 K, Lazaro J, Tybulewicz VLJ, Fisher EMC, Briscoe J. 2020. Species-specific pace of  
1255 development is associated with differences in protein stability. *Science (1979)* **369**.  
1256 doi:10.1126/science.aba7667
- 1257 Schreiber E, Matthias P, Müller MM, Schaffner W. 1989. Rapid detection of octamer binding  
1258 proteins with 'mini extracts', prepared from a small number of cells. *Nucleic Acids Res*  
1259 **17**:6419. doi:10.1093/nar/17.15.6419
- 1260 Scott EW, Simon MC, Anastasi J, Singh H. 1994. Requirement of transcription factor PU.1 in the  
1261 development of multiple hematopoietic lineages. *Science (1979)* **265**:1573–1577.  
1262 doi:10.1126/science.8079170
- 1263 Sergé A, Bertaux N, Rigneault H, Marguet D. 2008. Dynamic multiple-target tracing to probe  
1264 spatiotemporal cartography of cell membranes. *Nature Methods* **2008** *5*:8 **5**:687–694.  
1265 doi:10.1038/nmeth.1233
- 1266 Singh H, Dekoter RP, Walsh JC. 1999. PU.1, a Shared Transcriptional Regulator of Lymphoid  
1267 and Myeloid Cell Fates. *Cold Spring Harb Symp Quant Biol* **64**:13–20.  
1268 doi:10.1101/sqb.1999.64.13
- 1269 Springer T, Galfré G, Secher DS, Milstein C. 1979. Mac-1: a macrophage differentiation antigen  
1270 identified by monoclonal antibody. *Eur J Immunol* **9**:301–306. doi:10.1002/eji.1830090410
- 1271 Stoilova B, Kowenz-Leutz E, Scheller M, Leutz A. 2013. Lymphoid to Myeloid Cell Trans-  
1272 Differentiation Is Determined by C/EBP $\beta$  Structure and Post-Translational Modifications.  
1273 *PLoS One* **8**:e65169. doi:10.1371/journal.pone.0065169
- 1274 Suresh S, Huard S, Dubois T. 2021. CARM1/PRMT4: Making Its Mark beyond Its Function as a  
1275 Transcriptional Coactivator. *Trends Cell Biol* **31**:402–417. doi:10.1016/j.tcb.2020.12.010
- 1276 Teves SS, An L, Hansen AS, Xie L, Darzacq X, Tjian R. 2016. A dynamic mode of mitotic  
1277 bookmarking by transcription factors. *Elife* **5**. doi:10.7554/ELIFE.22280
- 1278 Torcal Garcia G, Graf T. 2021. The transcription factor code: a beacon for histone  
1279 methyltransferase docking. *Trends Cell Biol* **31**:792–800. doi:10.1016/j.tcb.2021.04.001
- 1280 Torres-Padilla ME, Parfitt DE, Kouzarides T, Zernicka-Goetz M. 2007. Histone arginine  
1281 methylation regulates pluripotency in the early mouse embryo. *Nature* **445**:214–218.  
1282 doi:10.1038/nature05458
- 1283 van Oevelen C, Collombet S, Vicent G, Hoogenkamp M, Lepoivre C, Badeaux A, Bussmann L,  
1284 Sardina JL, Thieffry D, Beato M, Shi Y, Bonifer C, Graf T. 2015. C/EBP $\alpha$  Activates Pre-

- 1285 existing and de Novo Macrophage Enhancers during Induced Pre-B Cell Transdifferentiation  
1286 and Myelopoiesis. *Stem Cell Reports* **5**:232–247. doi:10.1016/j.stemcr.2015.06.007
- 1287 Velten L, Haas SF, Raffel S, Blaszkiewicz S, Hennig BP, Hirche C, Lutz C, Buss EC, Boch T,  
1288 Hofmann W, Ho AD, Huber W. 2017. Human haematopoietic stem cell lineage commitment  
1289 is a continuous process **19**:271–281. doi:10.1038/ncb3493.Human
- 1290 Wang K, Wei G, Liu D. 2012. CD19: a biomarker for B cell development, lymphoma diagnosis  
1291 and therapy. *Exp Hematol Oncol* **1**:36. doi:10.1186/2162-3619-1-36
- 1292 Wang L, Zhao Z, Meyer MB, Saha S, Yu M, Guo A, Wisinski KB, Huang W, Cai W, Pike JW,  
1293 Yuan M, Ahlquist P, Xu W. 2014. CARM1 methylates chromatin remodeling factor BAF155  
1294 to enhance tumor progression and metastasis. *Cancer Cell* **25**:21–36.  
1295 doi:10.1016/j.ccr.2013.12.007
- 1296 Wu Q, Schapira M, Arrowsmith CH, Barsyte-Lovejoy D. 2021. Protein arginine methylation: from  
1297 enigmatic functions to therapeutic targeting. *Nat Rev Drug Discov* **20**:509–530.  
1298 doi:10.1038/s41573-021-00159-8
- 1299 Xie H, Ye M, Feng R, Graf T. 2004. Stepwise reprogramming of B cells into macrophages. *Cell*  
1300 **117**:663–676. doi:10.1016/S0092-8674(04)00419-2
- 1301 Xue HH, Bollenbacher-Reilley J, Wu Z, Spolski R, Jing X, Zhang YC, McCoy JP, Leonard WJ.  
1302 2007. The Transcription Factor GABP Is a Critical Regulator of B Lymphocyte Development.  
1303 *Immunity* **26**:421–431. doi:10.1016/j.jimmuni.2007.03.010
- 1304 Yadav N, Cheng D, Richard S, Morel M, Iyer VR, Aldaz CM, Bedford MT. 2008. CARM1  
1305 promotes adipocyte differentiation by coactivating PPAR $\gamma$ . *EMBO Rep* **9**:193–198.  
1306 doi:10.1038/sj.embo.7401151
- 1307 Zhang P, Iwasaki-Arai J, Iwasaki H, Fenyus ML, Dayaram T, Owens BM, Shigematsu H,  
1308 Levantini E, Huettner CS, Lekstrom-Himes JA, Akashi K, Tenen DG. 2004. Enhancement  
1309 of hematopoietic stem cell repopulating capacity and self-renewal in the absence of the  
1310 transcription factor C/EBP $\alpha$ . *Immunity* **21**:853–863. doi:10.1016/j.jimmuni.2004.11.006
- 1311 Zhang XK, Moussa O, LaRue A, Bradshaw S, Molano I, Spyropoulos DD, Gilkeson GS, Watson  
1312 DK. 2008. The Transcription Factor Fli-1 Modulates Marginal Zone and Follicular B Cell  
1313 Development in Mice. *The Journal of Immunology* **181**:1644–1654.  
1314 doi:10.4049/JIMMUNOL.181.3.1644
- 1315